NATIONAL AERONAUTICS AND SPACE ADMINISTRATION

TECHNICAL MEMORANDUM X-743

SUBSONIC AND SUPERSONIC AERODYNAMIC CHARACTERISTICS OF AN AIRPLANE CONFIGURATION UTILIZING DOUBLE-PIVOT VARIABLE-SWEEP WINGS*

By Edward C. Polhamus, William J. Alford, Jr., and Gerald V. Foster

SUMMARY

A variable-wing-sweep airplane having a double-inboard-pivot wing has been tested at low subsonic speeds and at a Mach number of 2.20 to determine the aerodynamic characteristics of this type of configuration. The double-pivot wing consists of a main wing and a fore wing, each pivoted within the fuselage in such a manner that unbroken leading and trailing edges are provided in both the low- and high-sweep positions. The results indicate that the variation of longitudinal stability with wing sweep angle for the double-pivot wing was similar to that of an outboard-pivot wing and considerably less than that of a single-inboard-pivot wing investigated in combination with the identical fuselage and tail arrangement. The total change in static margin due to increase in sweep of this wing from 25.00° to 71.50° and an increase in Mach number from 0.23 to 2.20 amounted to 11 percent of the mean aerodynamic chord of the 71.50° swept wing. At low speeds the double-pivot-wing configuration provided better longitudinal, directional, and lateral stability at high angles of attack than the outboard wing-pivot arrangement tested on the same airplane model.

INTRODUCTION

In order to provide data necessary for the design of airplanes capable of combining good subsonic and supersonic aerodynamic efficiency, the National Aeronautics and Space Administration is investigating various methods of applying the variable-sweep-wing concept. Most of the various schemes that have been proposed can be grouped into two categories: those that have the wing-sweep pivot located within the fuselage (referred to as inboard pivots) and those that have the pivot outside the fuselage in the wing (referred to as outboard pivots). The advantages of the inboard pivot are that sufficient structural depth is available to withstand the aerodynamic loads, and essentially unbroken leading edges are provided. The main disadvantage of the inboard pivot is the large aerodynamic-center shift with the wing sweep that requires either fore-and-aft translation of

*Title, Unclassified.

the wing or excessive control deflection. With the outboard pivot, the aerodynamic-center movement can be minimized; however, there are certain disadvantages such as the limited structural depth for the pivot and the broken leading edge for low sweep which gives rise to stability problems at high lift. The aerodynamic characteristics of configurations representative of both inboard- and outboard-pivot arrangements have been reported in references 1 to 6.

The results of preliminary studies made in an attempt to combine the advantages of the inboard- and outboard-pivot arrangements indicated that a configuration employing two pivots located within the fuselage should provide: adequate structural depth; an unbroken wing leading edge in both the high- and low-sweep positions, which would tend to eliminate the high-lift longitudinal instability generally associated with the outboard-pivot wings in the low-sweep position (refs. 1 and 2); and essentially the same level of longitudinal stability at a given Mach number for both the low-sweep and high-sweep wing positions.

In order to investigate further the characteristics of a double-pivot arrangement, airplane models with a main wing and a fore wing, each pivoted within the fuselage, were fabricated. An aerodynamic investigation of the models was made at subsonic speed (Mach number of 0.23) in the Langley 7- by 10-foot transonic tunnel and at supersonic speed (Mach number of 2.20) in the Langley 4- by 4-foot supersonic pressure tunnel. The results of the investigation are reported herein and the stability characteristics of the double-inboard-pivot arrangement are compared with those of outboard-pivot and single-inboard-pivot arrangements.

SYMBOLS

The forces and moments are referred to the body-axis system except for the lift and drag, which are referred to the wind axes (fig. 1). All coefficients are based on the geometric characteristics of the wing in the 71.50° sweep position. The moment-reference point was at fuselage station 36.08 inches for all configurations and sweep positions. The coefficients and symbols are defined as follows:

A	wing aspect ratio, b^2/S
b	wing span
C_D	drag coefficient, D/qS
C_L	lift coefficient, L/qS
C_l	rolling-moment coefficient, $\frac{\text{Rolling moment}}{qSb}$
C_{l_β}	effective-dihedral parameter, $\frac{\partial C_l}{\partial \beta}$

C_m pitching-moment coefficient, $\frac{\text{Pitching moment}}{qS\bar{c}}$

$C_{m_{C_L}}$ longitudinal-stability parameter, $\frac{\partial C_m}{\partial C_L}$

$C_{m_{i_t}}$ tail-effectiveness parameter, $\frac{\partial C_m}{\partial i_t}$

C_n yawing-moment coefficient, $\frac{\text{Yawing moment}}{qSb}$

C_{n_β} directional-stability parameter, $\frac{\partial C_n}{\partial \beta}$

C_Y lateral-force coefficient, $\frac{\text{Lateral force}}{qS}$

C_{Y_β} lateral-force parameter, $\frac{\partial C_Y}{\partial \beta}$

c local chord

$\bar{c}$ mean aerodynamic chord, $\frac{\int_0^{b/2} c^2 dy}{\int_0^{b/2} c\, dy}$

D drag

i_t horizontal-tail incidence, positive when trailing edge is down, deg

L lift

M free-stream Mach number

q free-stream dynamic pressure, $\frac{1}{2}\rho V^2$

S wing area

V free-stream velocity

y spanwise distance

α angle of attack, deg

β angle of sideslip, deg

Γ_t horizontal-tail dihedral angle, positive when tip is up, deg

Λ sweep angle of wing leading edge, deg

λ taper ratio

ρ mass density of air

DESCRIPTION OF MODELS

The models were representative of twin-engine attack airplanes and some two-view drawings are presented in figures 2 and 3. In order to compare the aerodynamic characteristics of the double-pivot wings with the outboard- and inboard-pivot wings on a consistent basis, the same fuselage and vertical-tail combination as used in reference 2 was employed. The configuration designations used herein are an extension of those used in reference 2; thus, the present models are referred to as configurations III, IV, and IV-A.

The sweptback wing ($\Lambda = 71.50^\circ$) of configuration III (fig. 2) was sized and located to approximate the 75° wing of configuration I (outboard pivot) of reference 2. In the low-sweep (25.00°) position the leading edge of the main wing of configuration III is approximately 2 inches farther forward than the outer wing panel of configuration I. To investigate the effect of wing longitudinal location, the low-sweep wing was moved rearward 2 inches and the resulting model is referred to as configuration IV (fig. 3). The horizontal tail used on both configurations III and IV was identical to that used in reference 2. For configuration IV, the effect of horizontal-tail dihedral angle was also studied. Configuration IV-A (fig. 3, dashed tail) utilized the same wing as configuration IV but the horizontal tail of IV-A was more highly swept, was located farther aft on the fuselage, and had approximately two-thirds as much exposed area as that of configuration IV. These alterations were made in an attempt to improve the match of the low-sweep wing and horizontal-tail contributions in order to provide linear pitching-moment variations with lift coefficient. For the 25.00° swept wing of configuration IV-A, the effects of a leading-edge chord extension were studied.

The wing airfoil section was identical to that of the outer panel of configuration I of reference 2; that is, an NACA 65A006 section parallel to the plane of symmetry with the wing in the 25° leading-edge-sweep position.

The operation of the double-pivot arrangement can best be described with the aid of figure 4, which shows photographs of configuration IV with the wing in three sweep positions. The top photograph shows the wing in the 25.00° sweep position with the main-wing pivots located at approximately the 40-percent-chord station and the fore-wing pivots located near the inlet lip. With the wing in the 25.00° sweep position the fore wing is retracted within the fuselage. As the main wing is swept back, the fore wing begins to emerge (center photograph of fig. 4) and when the 71.50° sweep position of the main wing is reached, the fore wing is fully extended and forms a straight leading edge (bottom photograph of fig. 4).

In addition to providing a continuous high-sweep leading edge, the lifting surface of the extended fore wing tends to offset the rearward shift in wing aerodynamic center relative to the aircraft center of gravity caused by the sweep of the main wing. It should be noted that the sweep-angle program of the fore wing can be arbitrarily chosen. The effects of changing the fore-wing sweep angle from 81.5° to 76° for configuration IV (fig. 3) with the main wing at the intermediate sweep angle of 48.25° were also investigated in the present study.

TESTS AND CORRECTIONS

The subsonic investigation was made in the Langley 7- by 10-foot transonic tunnel at a dynamic pressure of 75 lb/sq ft, corresponding to a Mach number of 0.23 and a Reynolds number per foot of approximately 1.65×10^6. This tunnel is an atmospheric tunnel with the upper and lower walls slotted longitudinally. No corrections are necessary for jet-boundary induced upwash or blockage in the slotted test section with models of this size.

The supersonic tests were made in the Langley 4- by 4-foot supersonic pressure tunnel at a Mach number of 2.20, a stagnation pressure of 1,008 lb/sq ft, and a stagnation temperature of 100° F. The corresponding Reynolds number was 1.58×10^6 per foot. The stagnation dewpoint was maintained sufficiently low (-25° or less) to avoid condensation effects in the test section.

The models were sting mounted to reduce support interference, and the forces and moments were measured with a six-component strain-gage balance. A photograph of one of the configurations mounted on the sting support in the Langley 7- by 10-foot transonic tunnel is shown as figure 5. In both tunnels the angles of attack and sideslip were corrected for the deflection of the sting and balance under load, the base pressure was measured and the drag adjusted to correspond to free-stream static pressure at the base, and the internal duct drag was measured and subtracted from the total drag. No sting-interference corrections have been applied to the data except that a partial correction for sting interference is inherent in the base-pressure correction. Transition was fixed on all surfaces with No. 100 carborundum grains.

PRESENTATION OF RESULTS

The basic data are presented in figures 6 to 25 and some of the more pertinent results are summarized in figures 26 and 27. As an aid in locating a particular portion of the basic data, the following table is presented:

Data	Figure numbers for configuration - III	IV	IV-A
Subsonic results (M = 0.23)			
Longitudinal aerodynamic characteristics			
Effect of sweep angle ($\Gamma_t = 0^\circ$, $i_t = 0^\circ$)	6	10	17
Effect of horizontal-tail deflection ($\Gamma_t = 0^\circ$)			
$\Lambda = 25.00^\circ$	7	11	18
$\Lambda = 48.25^\circ$	8	12	19
$\Lambda = 71.50^\circ$	9	13	20
Effect of fore-wing angle ($\Lambda = 48.25^\circ$, $\Gamma_t = 0^\circ$)		14	
Effect of sweep angle ($\Gamma_t = -20^\circ$, $i_t = 0^\circ$)		15	
Wing-off breakdown tests	16	16	
Effect of chord extension ($\Gamma_t = 0^\circ$, $i_t = 0^\circ$, $\Lambda = 25.00^\circ$)			21
Lateral aerodynamic characteristics ($\Gamma_t = 0^\circ$)			22
Supersonic results (M = 2.20)			
Longitudinal aerodynamic characteristics			
$\Lambda = 48.25^\circ$			24
$\Lambda = 71.50^\circ$		23	25

DISCUSSION

Subsonic Characteristics

An examination of the basic data to determine the effect of wing sweep-angle variation on the longitudinal aerodynamic characteristics (figs. 6, 10, and 17) indicates that the most desirable variation of pitching-moment coefficient with lift coefficient was obtained for configuration IV (fig. 10) in that the nonlinearities encountered were smaller and generally occurred at higher lift coefficients than for either configurations III or IV-A (figs. 6 and 17, respectively). In general, wing-sweep variation produced the same values of the lift-curve slope for configurations III and IV. For configuration IV-A the lift-curve slopes were approximately 13 percent less, throughout the sweep range, than for the other configurations. The maximum lift-drag ratios for configurations III and IV were approximately 10, 8, and 6 for sweep angles of 25.00°, 48.25°, and 71.50°, respectively. For configuration IV-A the maximum lift-drag ratios were higher by approximately $2\frac{1}{2}$ percent at 25.00° sweep and by 10 percent at 71.50° sweep. The reduction in lift-curve slope and increase in lift-drag ratios are the result of the smaller horizontal-tail area of configuration IV-A.

At constant angle of attack the horizontal-tail effectiveness parameter $C_{m_{i_t}}$ was essentially constant throughout the sweep range for all configurations. For configurations III (figs. 7, 8, and 9) and IV (figs. 11, 12, and 13), the tail

effectiveness was essentially the same when the appropriate reference areas and chords are considered. This fact indicates that wing location had no appreciable effect on tail effectiveness. For configuration IV-A (figs. 18, 19, and 20), the decrease in tail volume due to the decrease in tail area and increase in tail sweep caused a reduction in the tail effectiveness. For all configurations investigated the tail effectiveness appears sufficient to provide trim throughout the usable lift-coefficient range.

The effect of changing the fore-wing sweep angle for an intermediate main-wing sweep angle ($\Lambda = 48.25^\circ$) is shown in figure 14 for configuration IV. For comparison, the effect of removing the fore wing is also included. The only significant result of the decrease in the fore-wing sweep angle is the destabilizing effect due to the increased area ahead of the moment-reference point.

Changing the horizontal-tail dihedral angle of configuration IV from 0° (fig. 10) to -20° (fig. 15) had no effect other than to accentuate the instability occurring at the higher lift coefficients for the 71.50° swept wing.

The addition of a leading-edge chord extension to the 25.00° swept wing of configuration IV-A provided sizable increases in lift coefficient and lift-drag ratio for angles of attack between 10° and 16° (fig. 21).

The lateral characteristics of configuration IV-A shown in figure 22 indicate that this configuration is directionally stable throughout the angle-of-attack range investigated. The configuration becomes increasingly stable, at the higher angles of attack, as the wing sweep angle is increased. The same observations are applicable to the lateral stability as indicated by the effective-dihedral parameter $-C_{l_\beta}$.

Supersonic Characteristics

A comparison of the results for the 71.50° sweep condition of configuration IV (fig. 23) and configuration IV-A (fig. 25) indicates that the effect of the tail planform is negligible at $M = 2.20$ in that all longitudinal results are identical. Inasmuch as the Reynolds numbers for the subsonic and supersonic tests are comparable, it is interesting to note that the maximum lift-drag ratios for the 71.50° sweep have decreased from approximately 6.6 at $M = 0.23$ (fig. 17) to 5.0 at $M = 2.20$ (fig. 25), whereas the lift-drag ratio for the intermediate wing sweep (fig. 24) is about 4.3 since for this sweep the wing leading edge is supersonic. As would be expected, the longitudinal-stability parameter $\partial C_m/\partial C_L$ has increased negatively, compared with the subsonic value, and is approximately -0.20 for the 48.25° sweep angle (fig. 24) and -0.19 for the 71.50° sweep angle (fig. 25).

Stability Characteristics of Different Wing-Pivot Arrangements

For comparing the stability characteristics of the double-pivot arrangement with the inboard- and outboard-pivot arrangements of reference 2, configuration IV of the present study was chosen inasmuch as it provided the most desirable variations with lift coefficient and angle of attack.

Figure 26 presents the variation of static margin $C_{m_{C_L}}$ with wing sweep position for configuration IV and, for comparison, configurations I and II of reference 2. The dashed curves between the extreme sweep positions for configuration I were obtained from unpublished results for the same wing on a slightly different fuselage. For configuration IV with the main wing swept 48.25°, tail-on data are given for the fore wing in three positions: basic (81.5°), completely retracted (off), and extended to a greater degree (swept 76°) than the basic. These three conditions represent various sweep scheduling of the fore wing relative to the main wing. The data illustrate the degree to which the fore wing might be used to control the static margin during the sweep transition or for flight at intermediate sweep positions. The results in figure 26 indicate that the double pivot limits the stability variation to a considerably greater degree than the single inboard pivot and is quite similar in effectiveness to the outboard pivot. The overall increase in static margin between the 25.00° sweep position and the 71.50° sweep position is only 4 percent of the mean aerodynamic chord of the 71.50° wing, and the additional increase associated with an increase in Mach number to 2.20 (fig. 23) is approximately 7 percent. Thus, the overall increase in static margin between the model with low sweep at low speed and the model with 71.50° sweep at $M = 2.20$ is only about 11 percent $\bar{c}$.

In order to assess fully the static stability of the double-pivot wing for subsonic speeds, its characteristics throughout the lift-coefficient range must be considered. Figure 27, therefore, presents the longitudinal, directional, and lateral stability characteristics throughout the lift-coefficient or angle-of-attack range for the high- and low-sweep positions of the double-pivot wing of the present investigation and, for comparison, the corresponding characteristics of the outboard-pivot wing of reference 2. Regarding the longitudinal stability characteristics, the advantage of the double pivot in avoiding the discontinuous or broken leading edge in the low-sweep position can be seen in the fact that whereas the outboard-pivot wing exhibited a pitchup, the stability of the double-pivot wing gradually increased with increasing lift coefficient. The double-pivot wing should therefore allow considerably more leeway with regard to horizontal-tail vertical location and wing-airfoil camber or leading-edge devices. For the high-sweep position the double-pivot wing exhibits a loss in stability at the higher lift coefficients; however, under normal conditions the aircraft would not be operating at low speeds with the wing in this position.

The directional-stability results C_{n_β} in figure 27 indicate that the reduction in directional stability occurs at considerably higher angles of attack with the double-pivot wing. The improvement for the low-sweep case is probably due to the elimination of the highly swept inner panel of the outboard-pivot wing which would tend to induce unfavorable sidewash on the tail at moderate and high angles of attack. The improvement at the high-sweep position may be associated with outboard displacements of the wing leading-edge separation vortex and the reduction or elimination of the cross-flow separation vortex that originates in the region of the inlet duct for configuration I of reference 2, as the fore wing of the present study also originates at the inlet duct.

Improvements in the lateral stability, as indicated by the variation of the effective-dihedral parameter $-C_{l_\beta}$ with angle of attack, are evident for the

double-pivot wing in both the high- and low-sweep positions (fig. 27). The greatest improvement is for the 25.00° sweep position and is due to the improvement in the flow on the outer wing panel associated with the elimination of the high-sweep fore wing, which presumably induced large upwash angles on the outer wing panels and thereby caused flow separation at the highest angles of attack.

CONCLUDING REMARKS

The aerodynamic characteristics of a variable-sweep configuration with a double-pivot wing have been investigated at low subsonic and supersonic speeds. The variation of longitudinal stability with wing sweep angle for the double-pivot wing was similar to that for an outboard-pivot wing and considerably less than that for a single-inboard-pivot wing investigated in combination with the identical fuselage-tail arrangement. The total change in static margin due to increase in sweep of the wing from 25.00° to 71.50° and increase in Mach number from 0.23 to 2.20 amounted to 11 percent of the mean aerodynamic chord of the 71.50° swept wing. At low speeds the double-pivot wing provided better longitudinal, directional, and lateral stability at high angles of attack than the outboard wing-pivot arrangements tested on the same airplane model.

Langley Research Center,
National Aeronautics and Space Administration,
Langley Station, Hampton, Va., September 19, 1962.

REFERENCES

1. Alford, William J., Jr., and Henderson, William P.: An Exploratory Investigation of the Low-Speed Aerodynamic Characteristics of Variable-Wing-Sweep Airplane Configurations. NASA TM X-142, 1959.

2. Spencer, Bernard, Jr.: Stability and Control Characteristics at Low Subsonic Speeds of an Airplane Configuration Having Two Types of Variable-Sweep Wings. NASA TM X-303, 1960.

3. Foster, Gerald V., and Morris, Odell A.: Stability and Control Characteristics at a Mach Number of 1.97 of an Airplane Configuration Having Two Types of Variable-Sweep Wings. NASA TM X-323, 1960.

4. Bielat, Ralph P., Robins, A. Warner, and Alford, William J., Jr.: The Transonic Aerodynamic Characteristics of Two Variable-Sweep Airplane Configurations Capable of Low-Level Supersonic Attack. NASA TM X-304, 1960.

5. Spearman, M. Leroy, and Robinson, Ross B.: Stability and Control Characteristics at a Mach Number of 2.01 of a Variable-Sweep Airplane Configuration Capable of Low-Level Supersonic Attack - Outer Wing Swept 75°. NASA TM X-310, 1960.

6. Polhamus, Edward C., and Hammond, Alexander D.: Aerodynamic Research Relative to Variable-Sweep Multimission Aircraft. Ch. II of Compilation of Papers Summarizing Some Recent NASA Research on Manned Military Aircraft. NASA TM X-420, 1960, pp. 13-38.

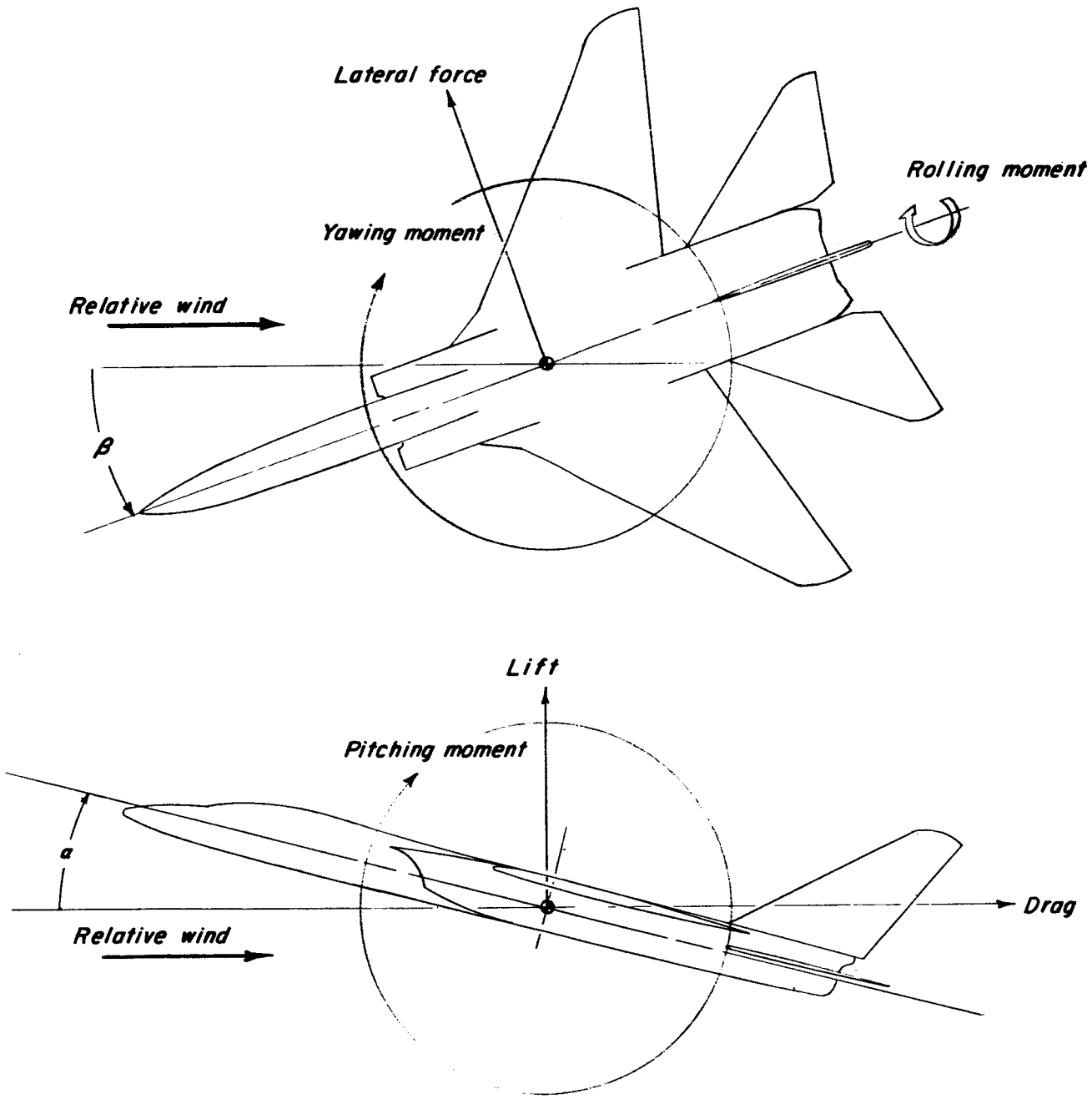

Figure 1.- System of axes used, showing the positive direction of forces, moments, and angles.

$\Lambda_{LE} = 25.00°$	$\Lambda_{LE} = 48.25°$	$\Lambda_{LE} = 71.50°$
$S = 2.37\ ft^2$	$S = 3.00\ ft^2$	$S = 3.25\ ft^2$
$\bar{c} = 7.77$	$\bar{c} = 13.61$	$\bar{c} = 18.65$
$b = 51.36$	$b = 43.62$	$b = 30.36$
$A = 7.71$	$A = 4.41$	$A = 1.97$
$\lambda = .17$		

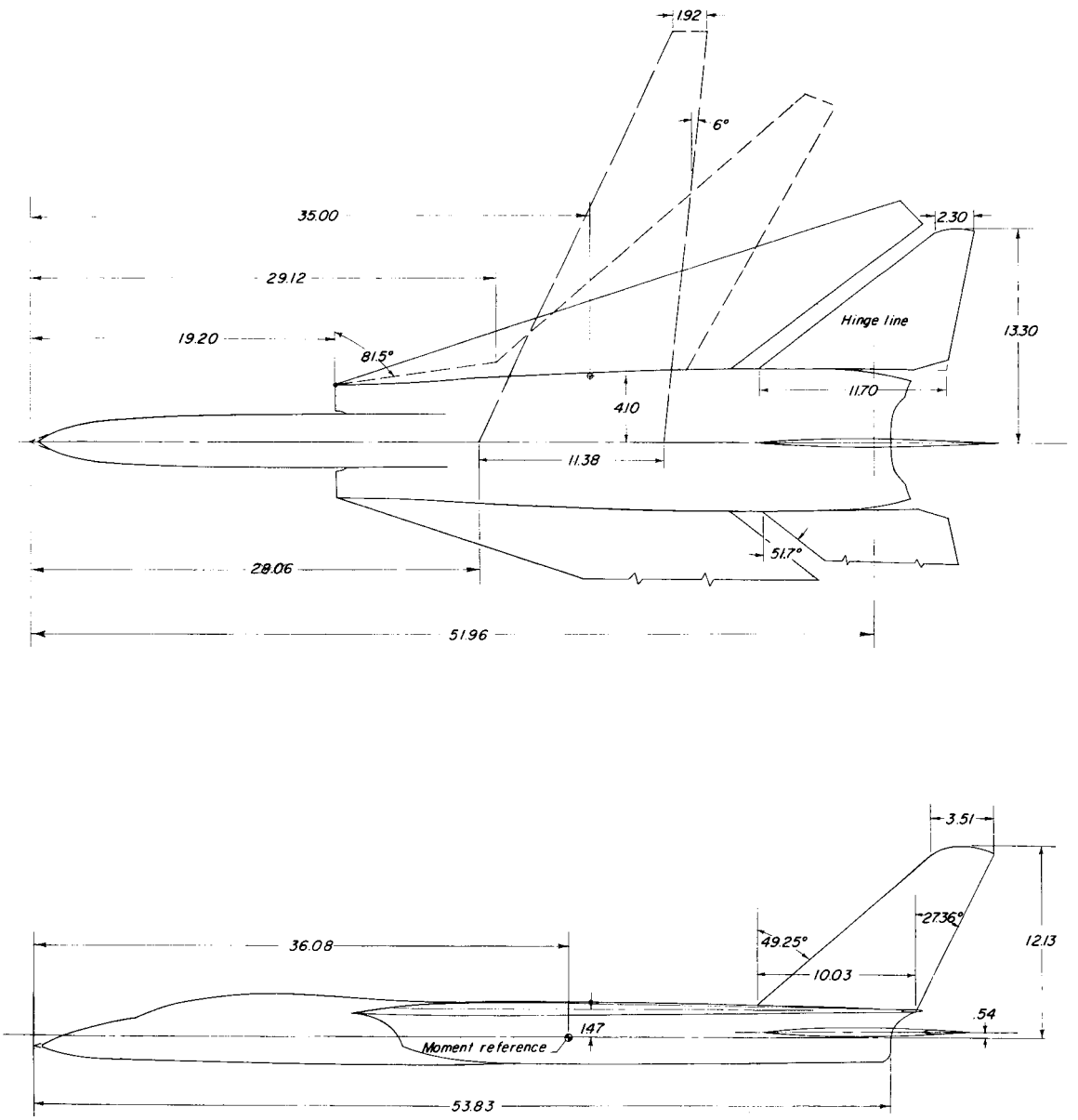

Figure 2.- Details of configuration III. All dimensions are in inches unless otherwise indicated.

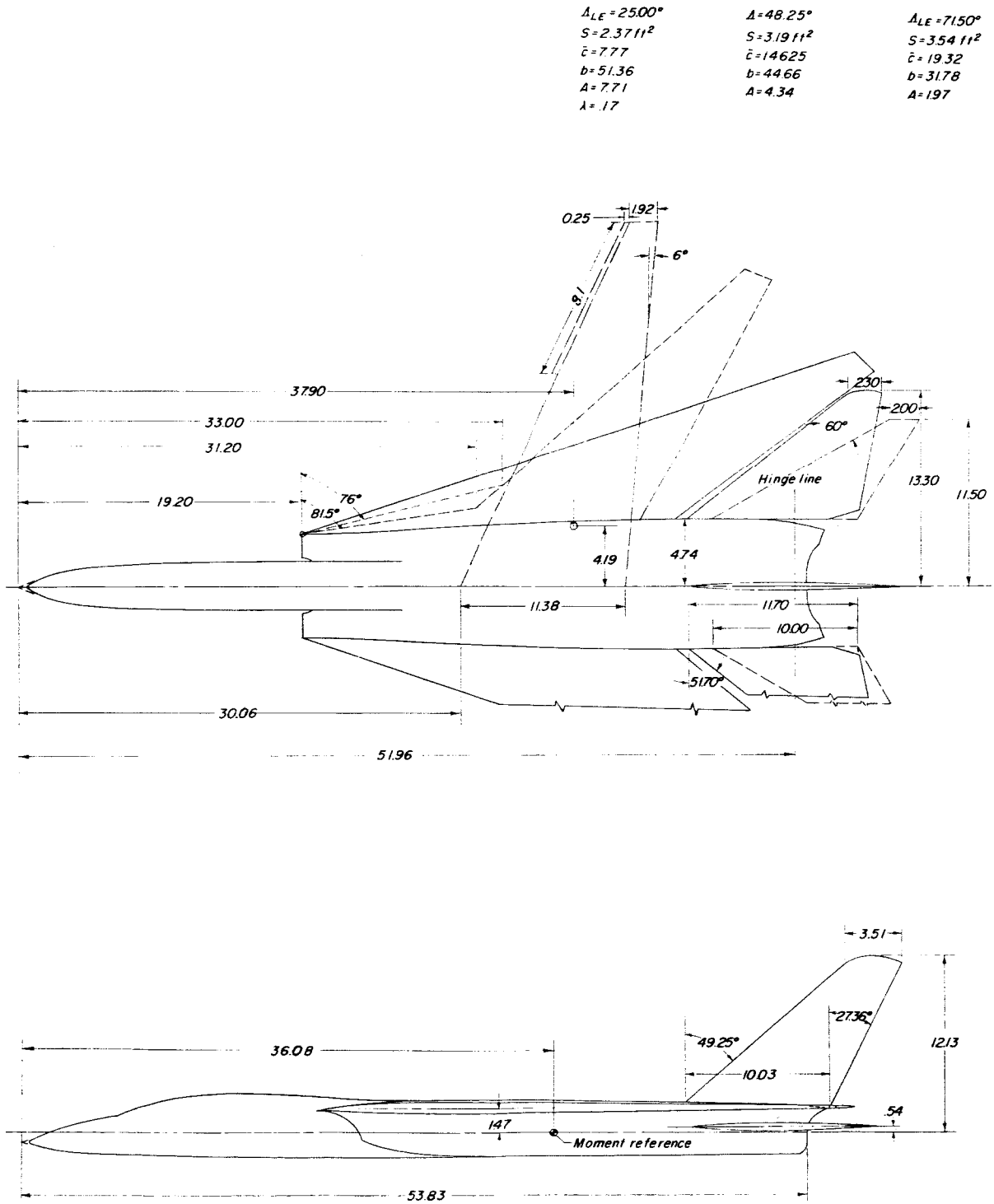

Figure 3.- Details of configurations IV and IV-A (IV-A represented by dashed tail). All dimensions are in inches unless otherwise indicated.

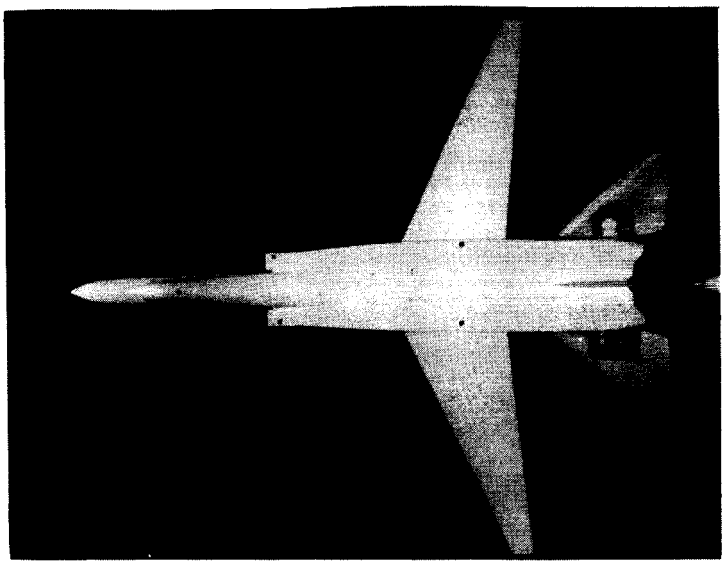

Λ = 25.00°

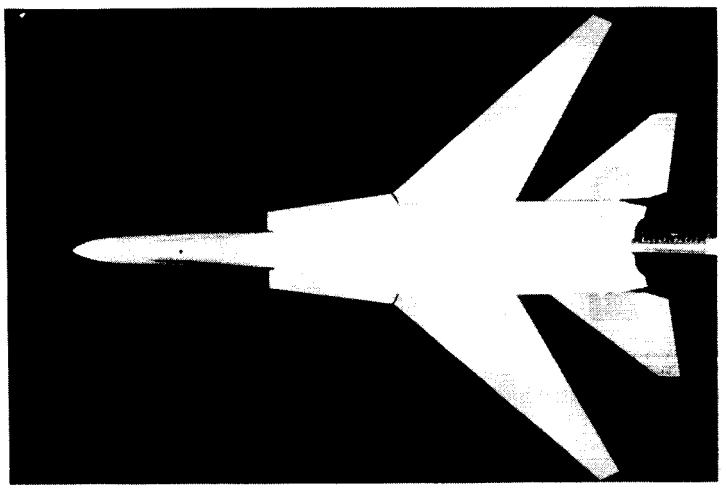

Λ = 48.25°

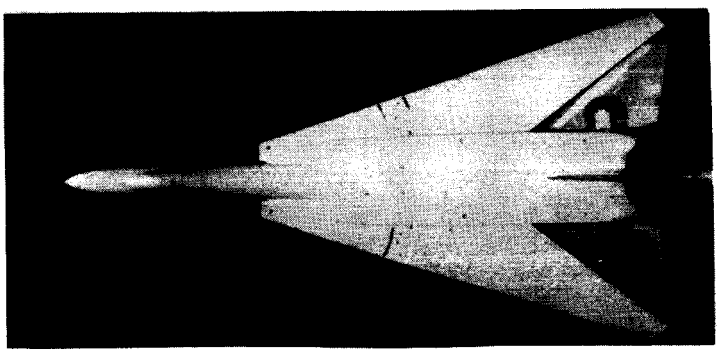

Λ = 71.50°

L-62-7017

Figure 4.- Photographs of configuration IV at three sweep positions.

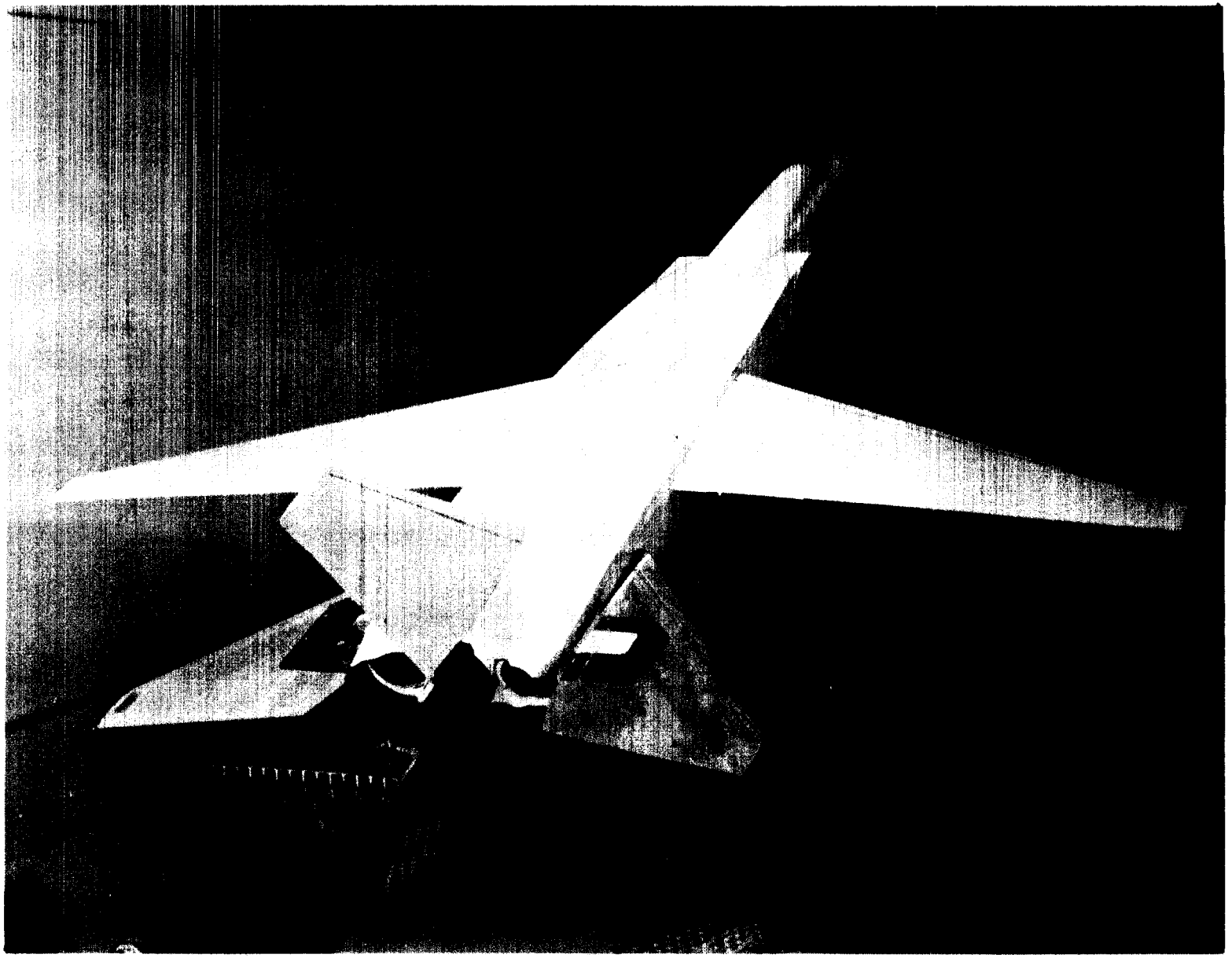

L-61-456

Figure 5.- Photograph of model mounted on sting support in Langley 7- by 10-foot transonic tunnel.

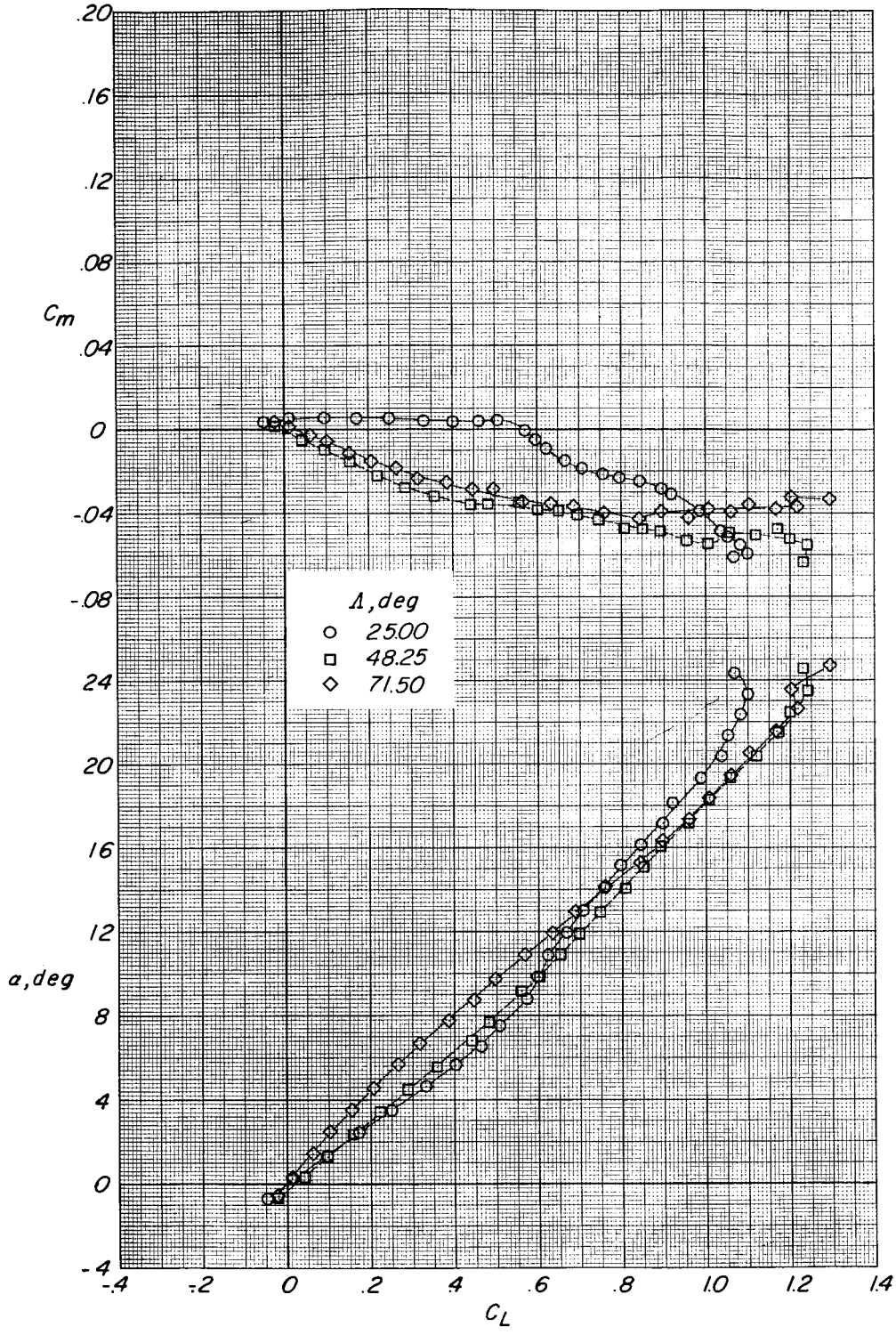

Figure 6.- Effect of wing sweep angle on subsonic longitudinal aerodynamic characteristics of configuration III. $\Gamma_t = 0^\circ$; $i_t = 0^\circ$; M = 0.23.

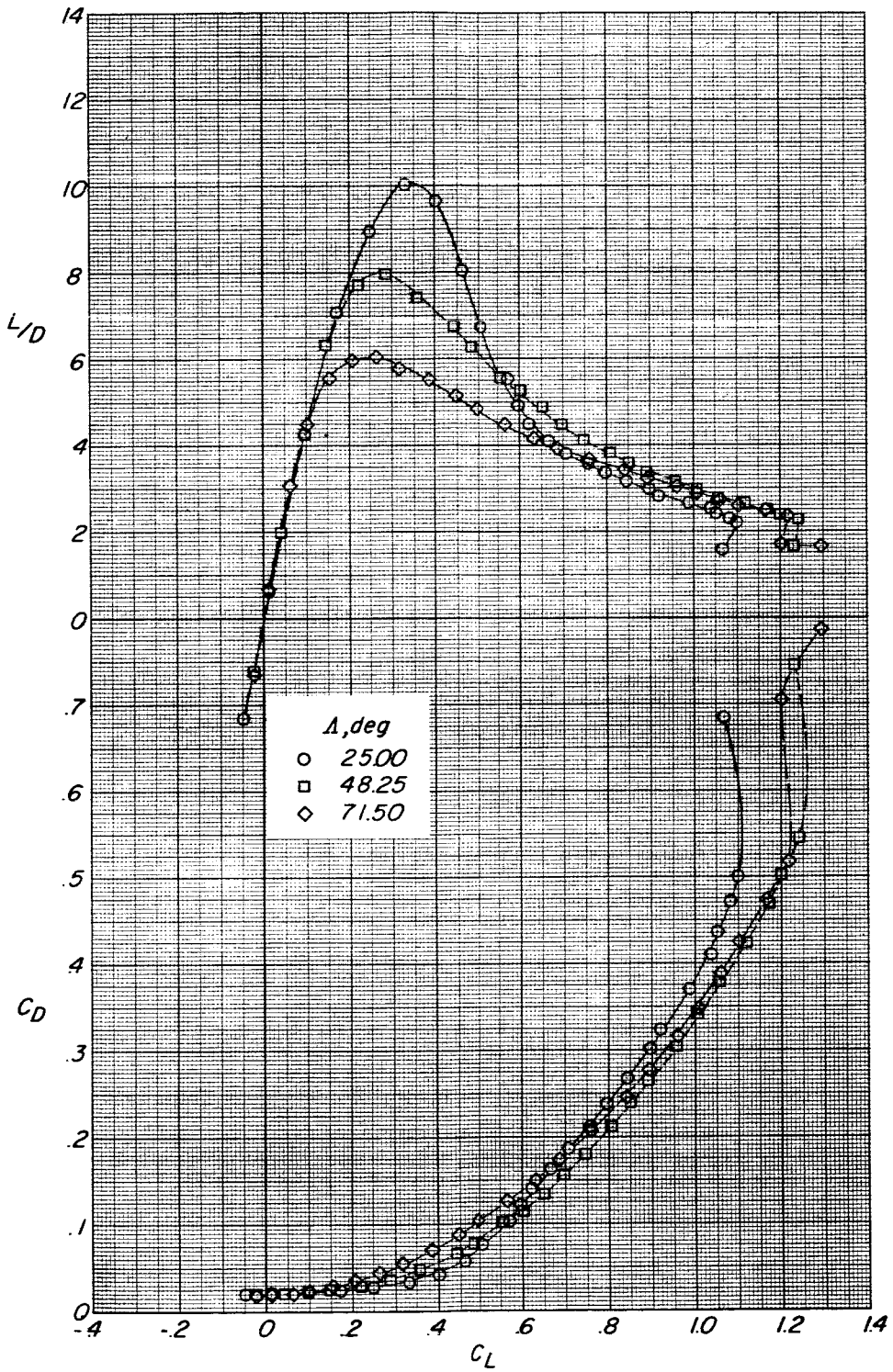

Figure 6.- Concluded.

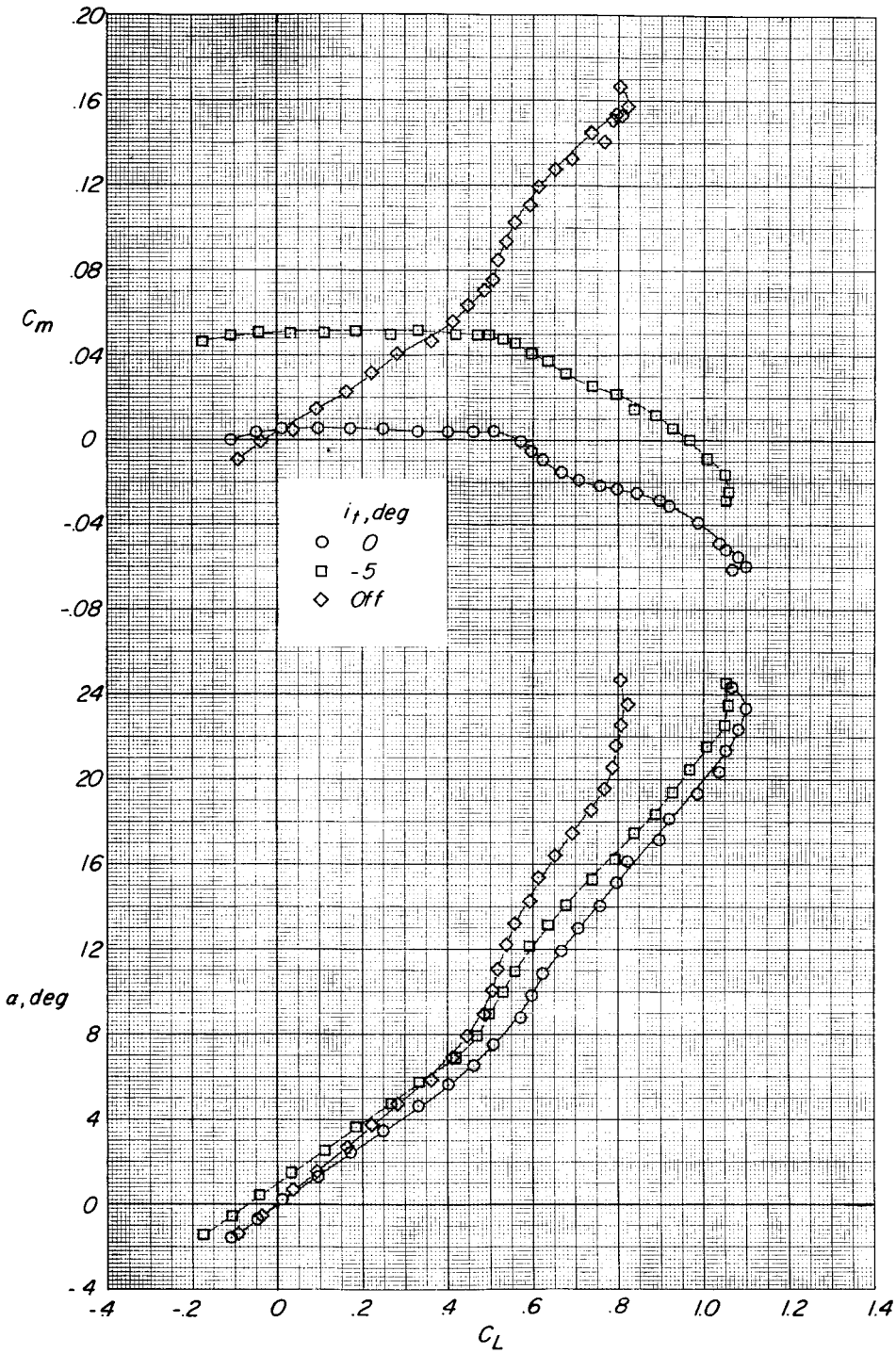

Figure 7.- Effect of horizontal-tail deflection on subsonic longitudinal aerodynamic characteristics of configuration III with $\Lambda = 25.00^{\circ}$. $\Gamma_t = 0^{\circ}$; M = 0.23.

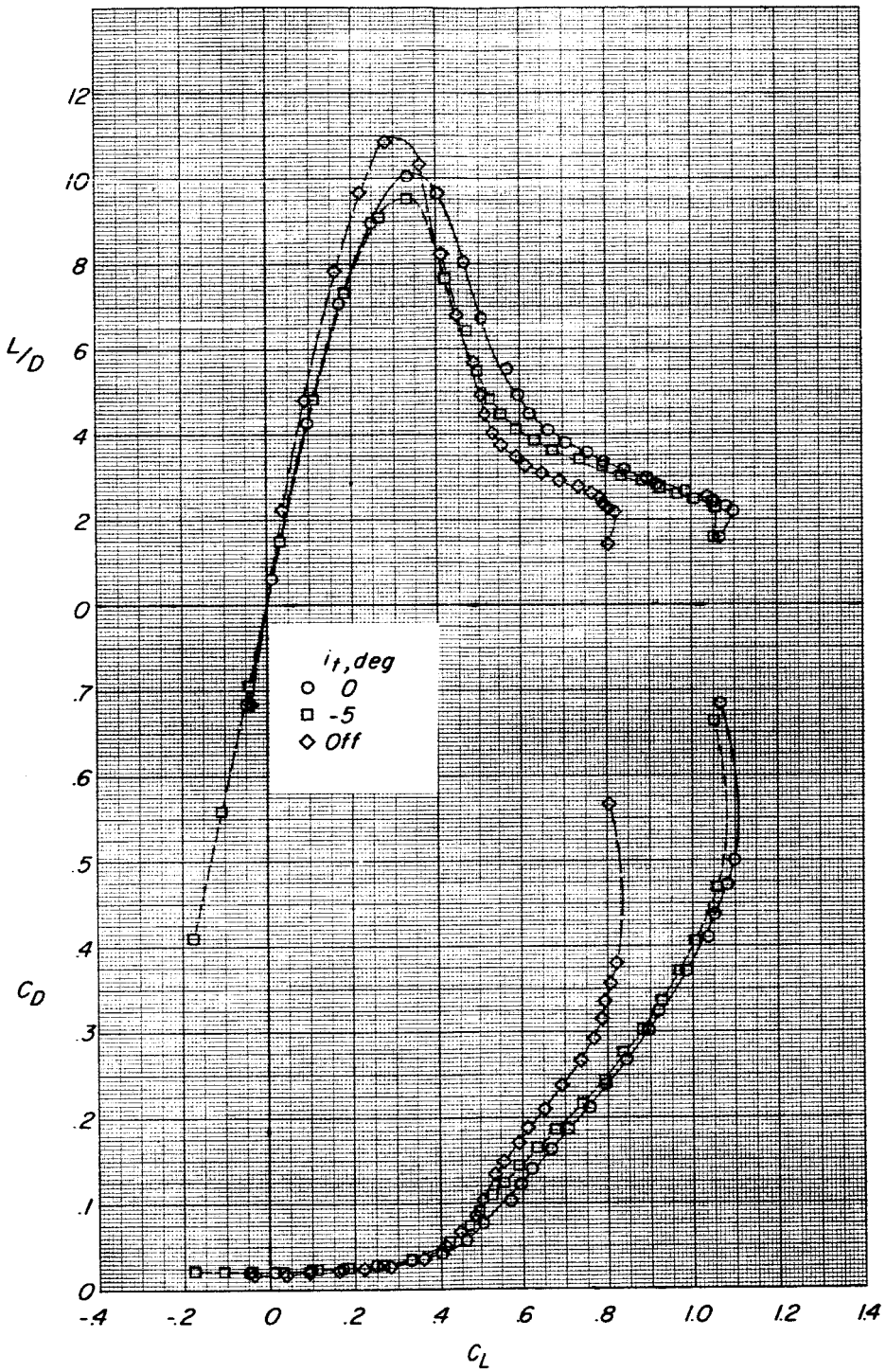

Figure 7.- Concluded.

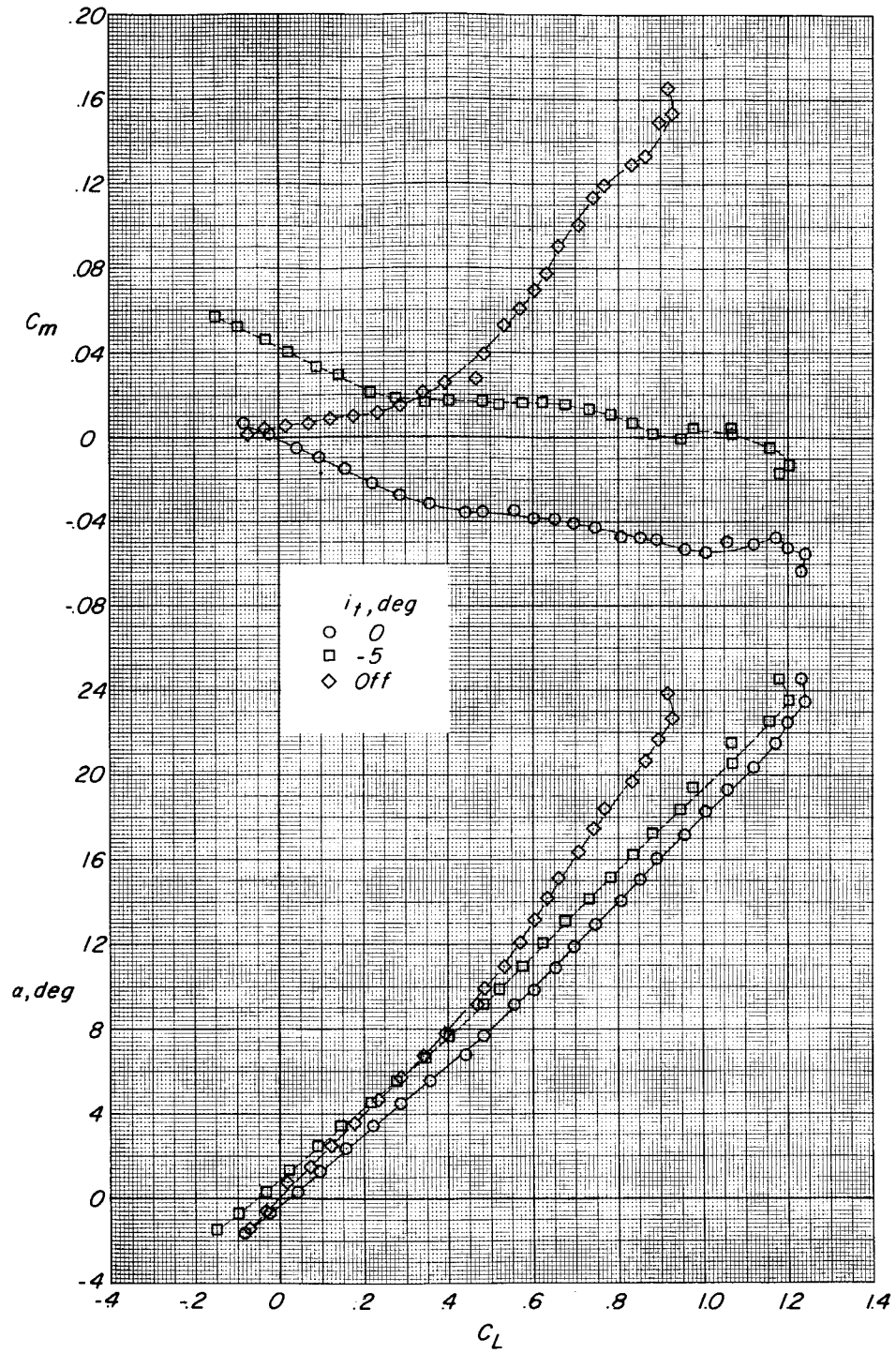

Figure 8.- Effect of horizontal-tail deflection on subsonic longitudinal aerodynamic characteristics of configuration III with $\Lambda = 48.25^\circ$. $\Gamma_t = 0^\circ$; M = 0.23.

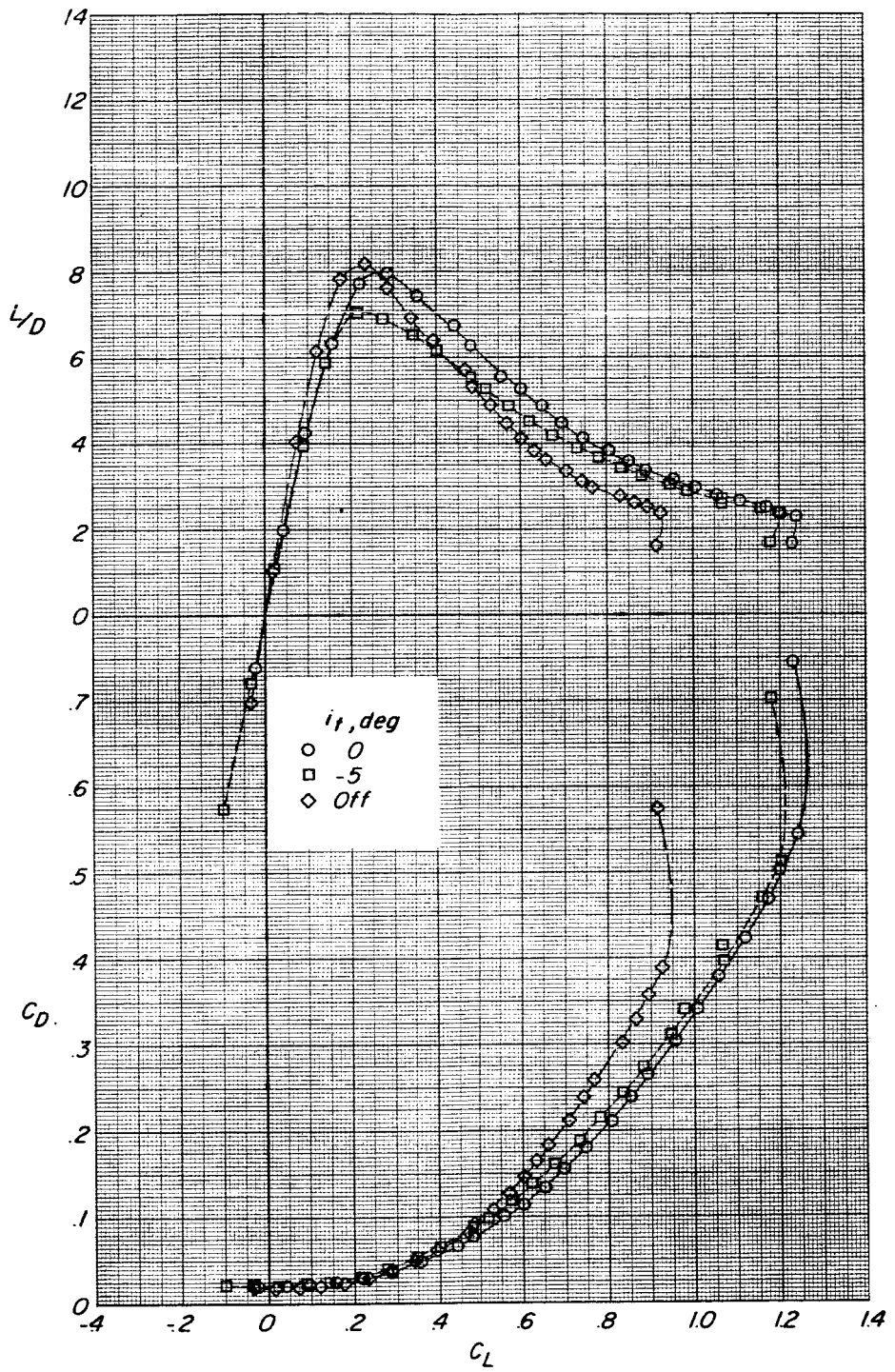

Figure 8.- Concluded.

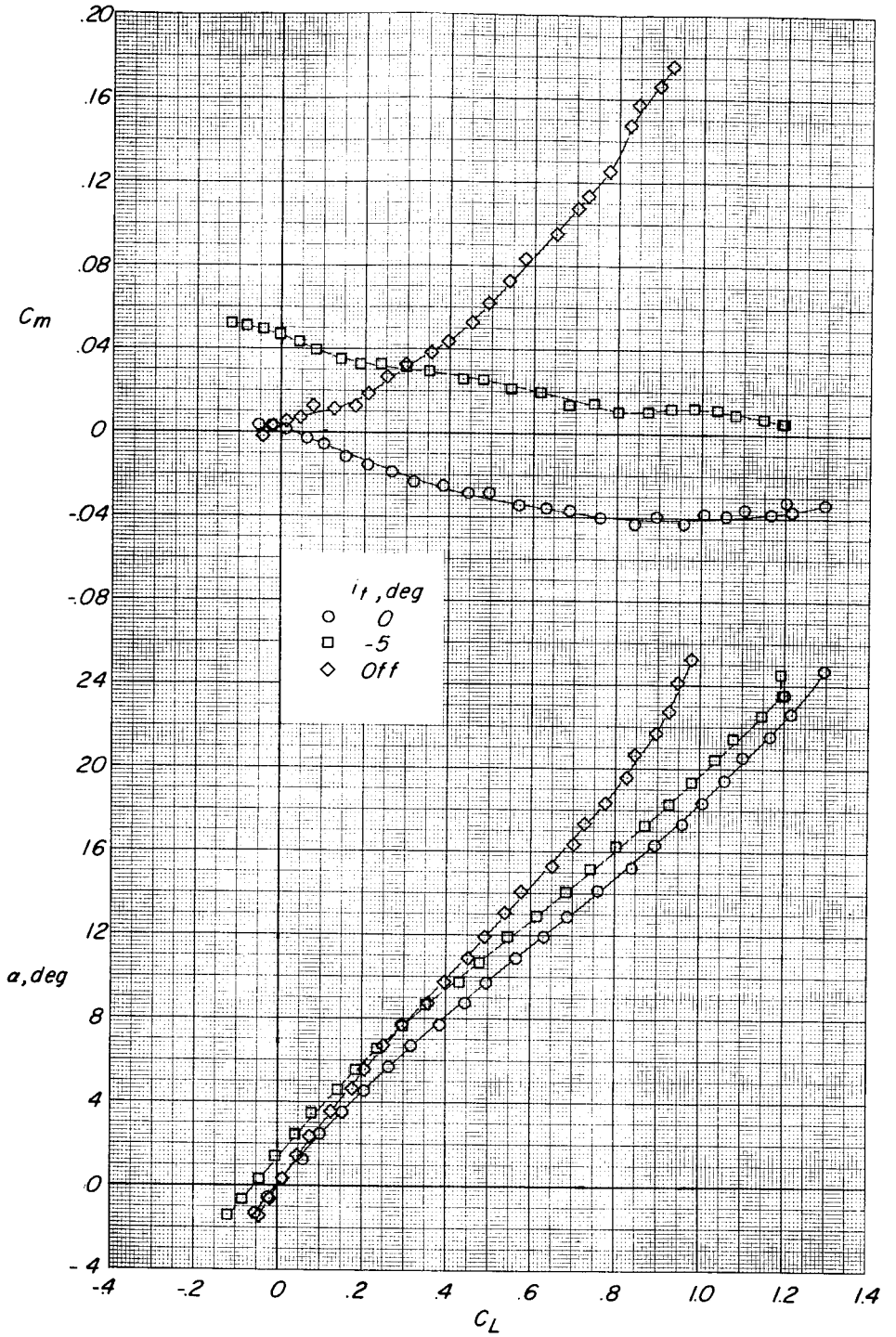

Figure 9.- Effect of horizontal-tail deflection on subsonic longitudinal aerodynamic characteristics of configuration III with $\Lambda = 71.50^{\circ}$. $\Gamma_t = 0^{\circ}$; M = 0.23.

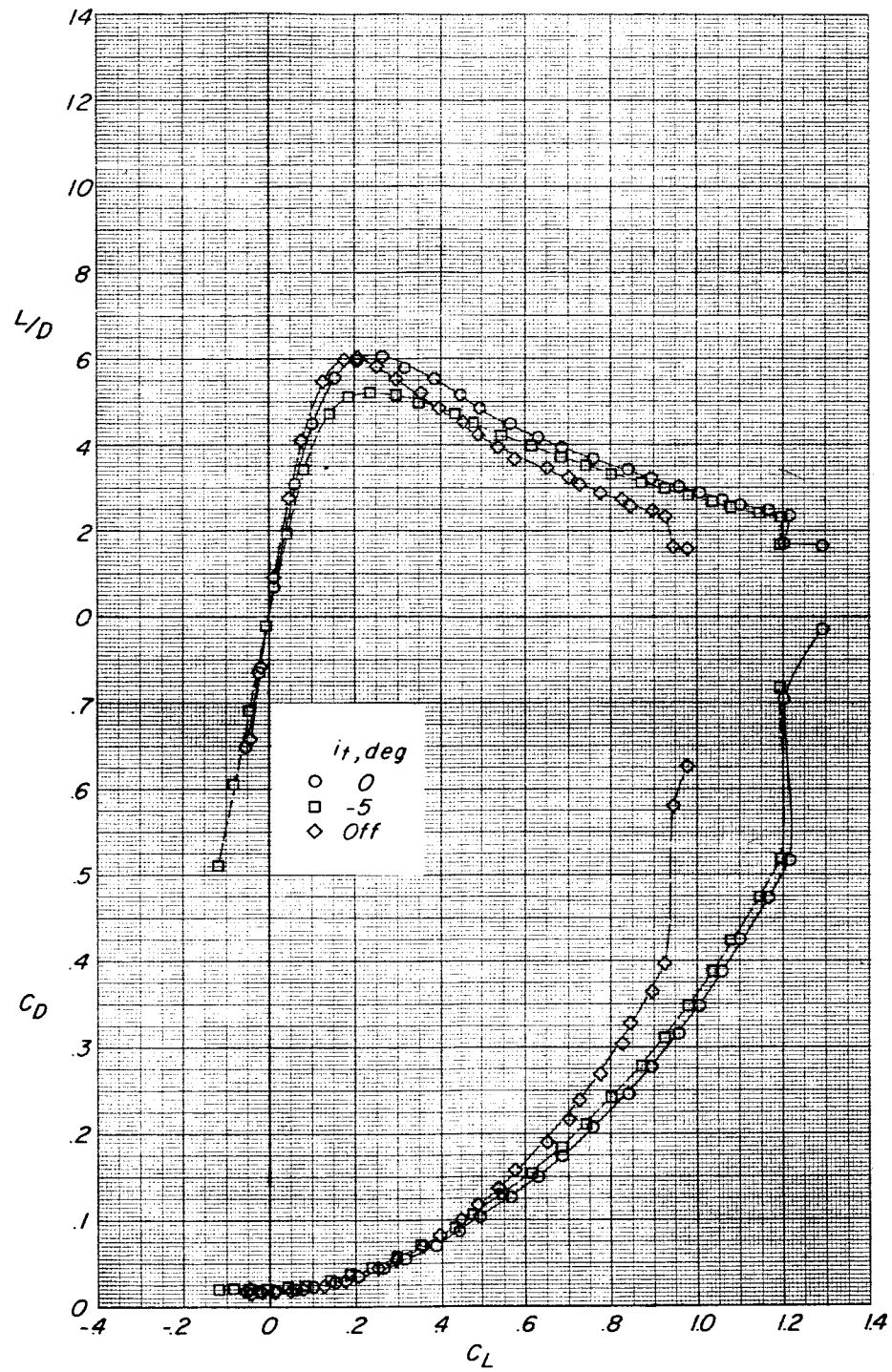

Figure 9.- Concluded.

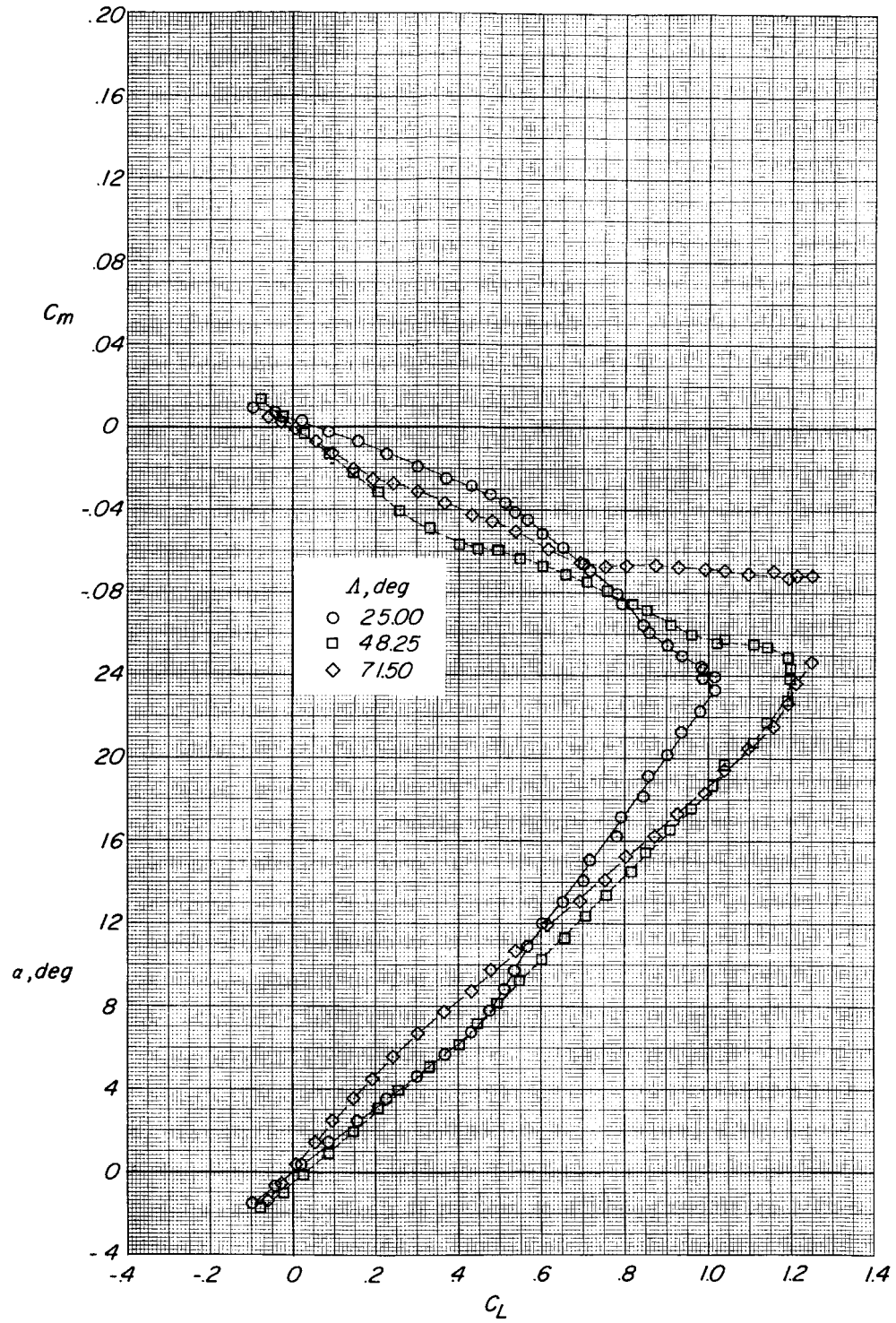

Figure 10.- Effect of wing sweep angle on subsonic longitudinal aerodynamic characteristics of configuration IV. $\Gamma_t = 0^\circ$; $i_t = 0^\circ$; M = 0.23.

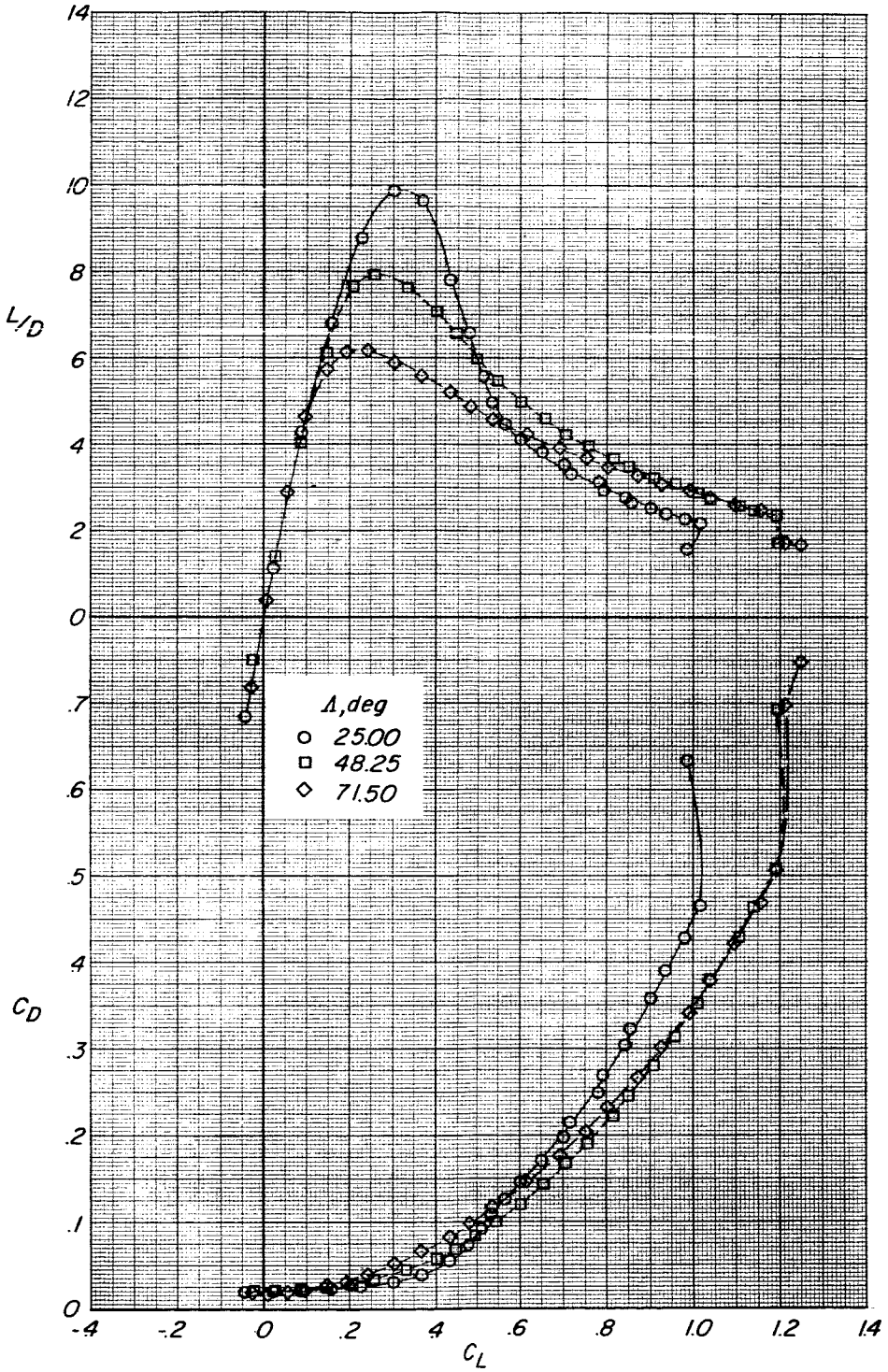

Figure 10.- Concluded.

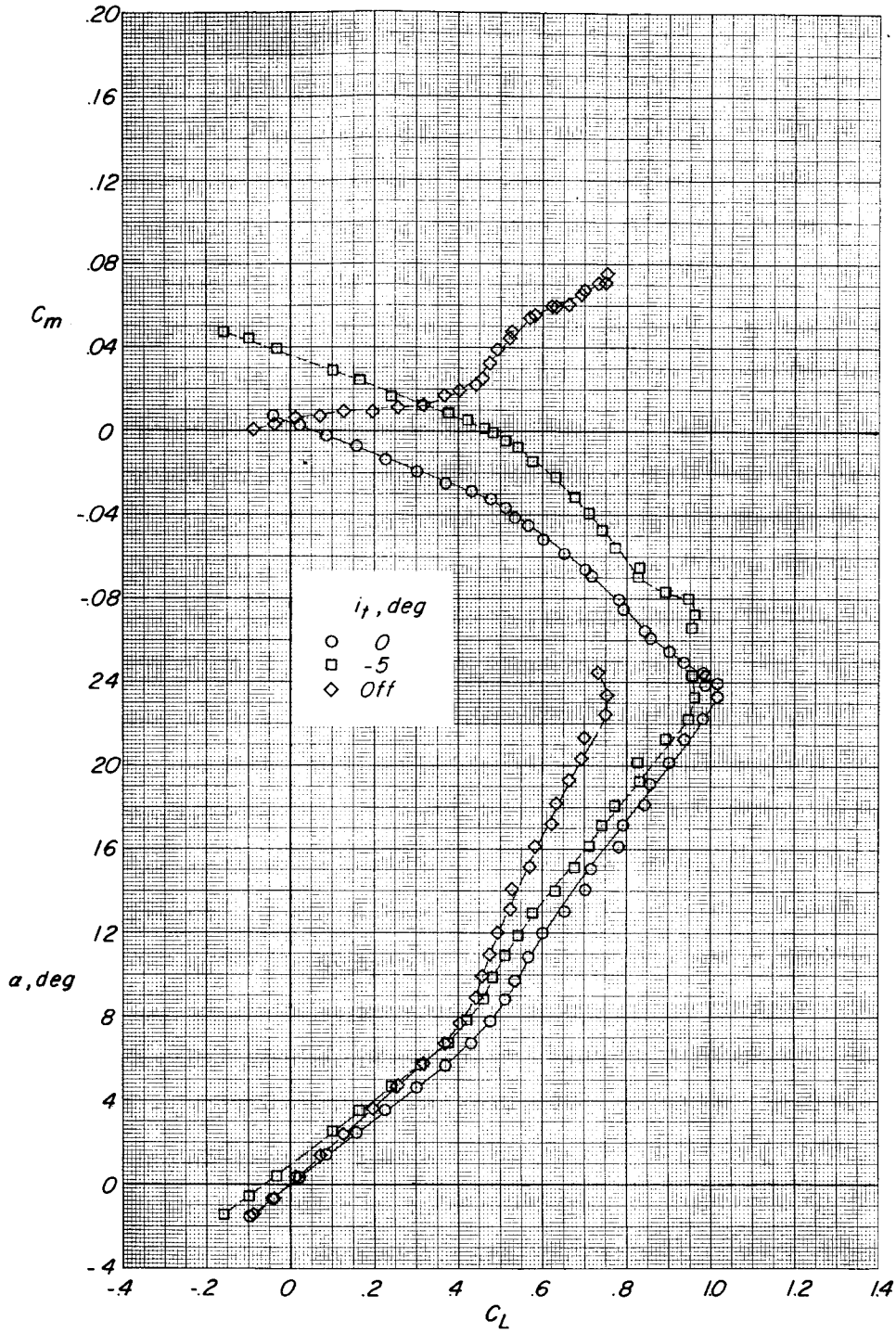

Figure 11.- Effect of horizontal-tail deflection on subsonic longitudinal aerodynamic characteristics of configuration IV with $\Lambda = 25.00^{\circ}$. $\Gamma_t = 0^{\circ}$; M = 0.23.

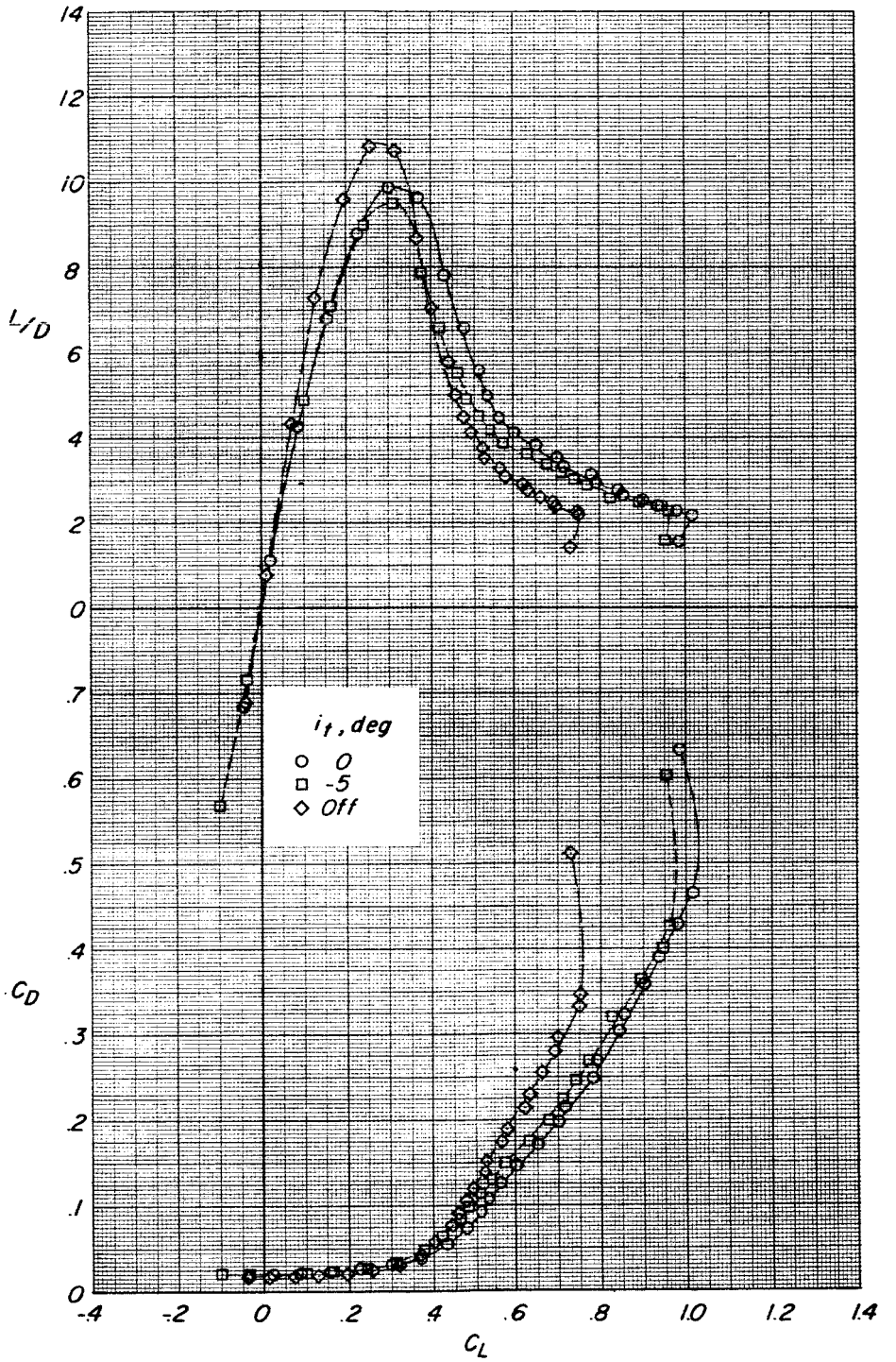

Figure 11.- Concluded.

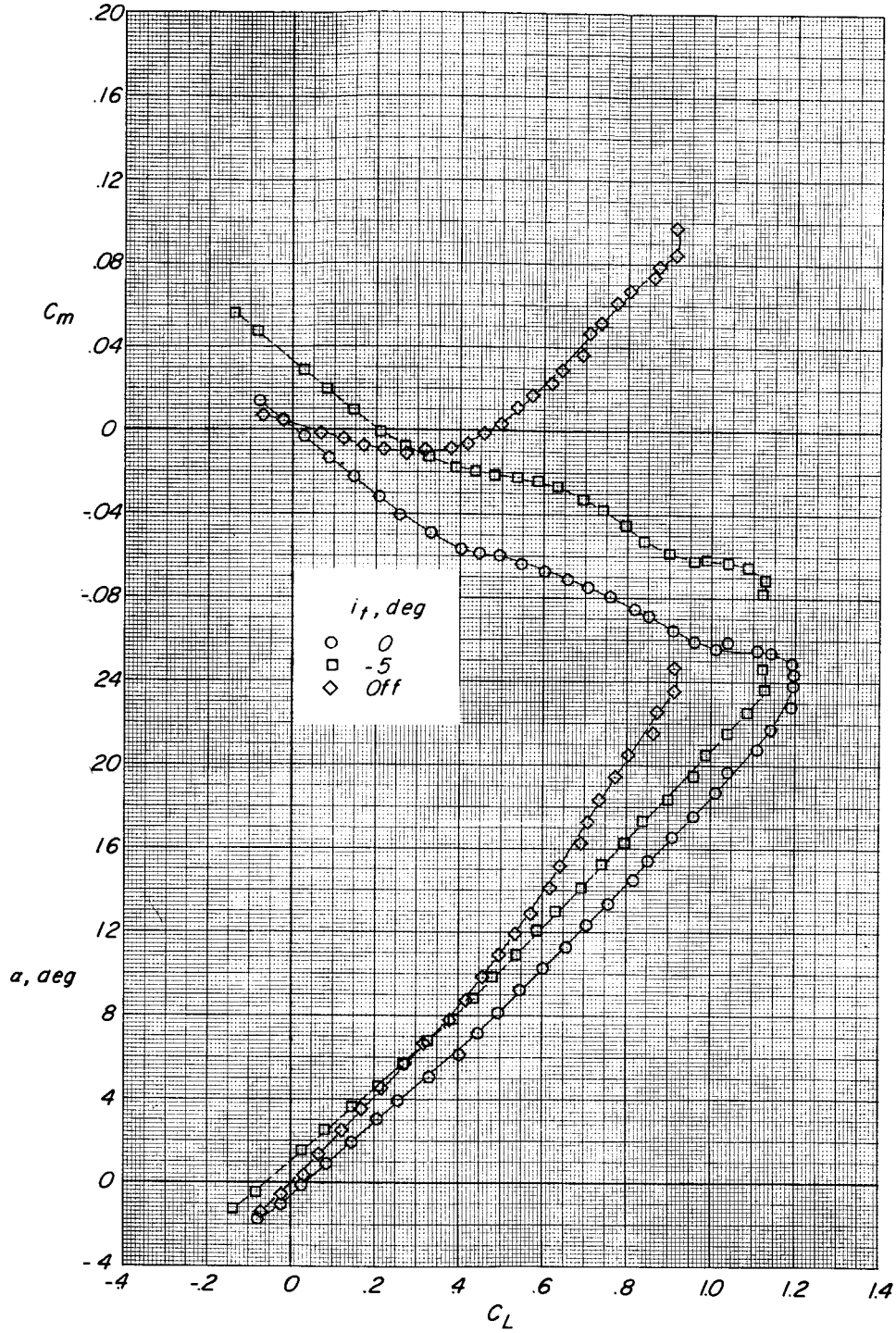

Figure 12.- Effect of horizontal-tail deflection on subsonic longitudinal aerodynamic characteristics of configuration IV with $\Lambda = 48.25^\circ$. $\Gamma_t = 0^\circ$; M = 0.23.

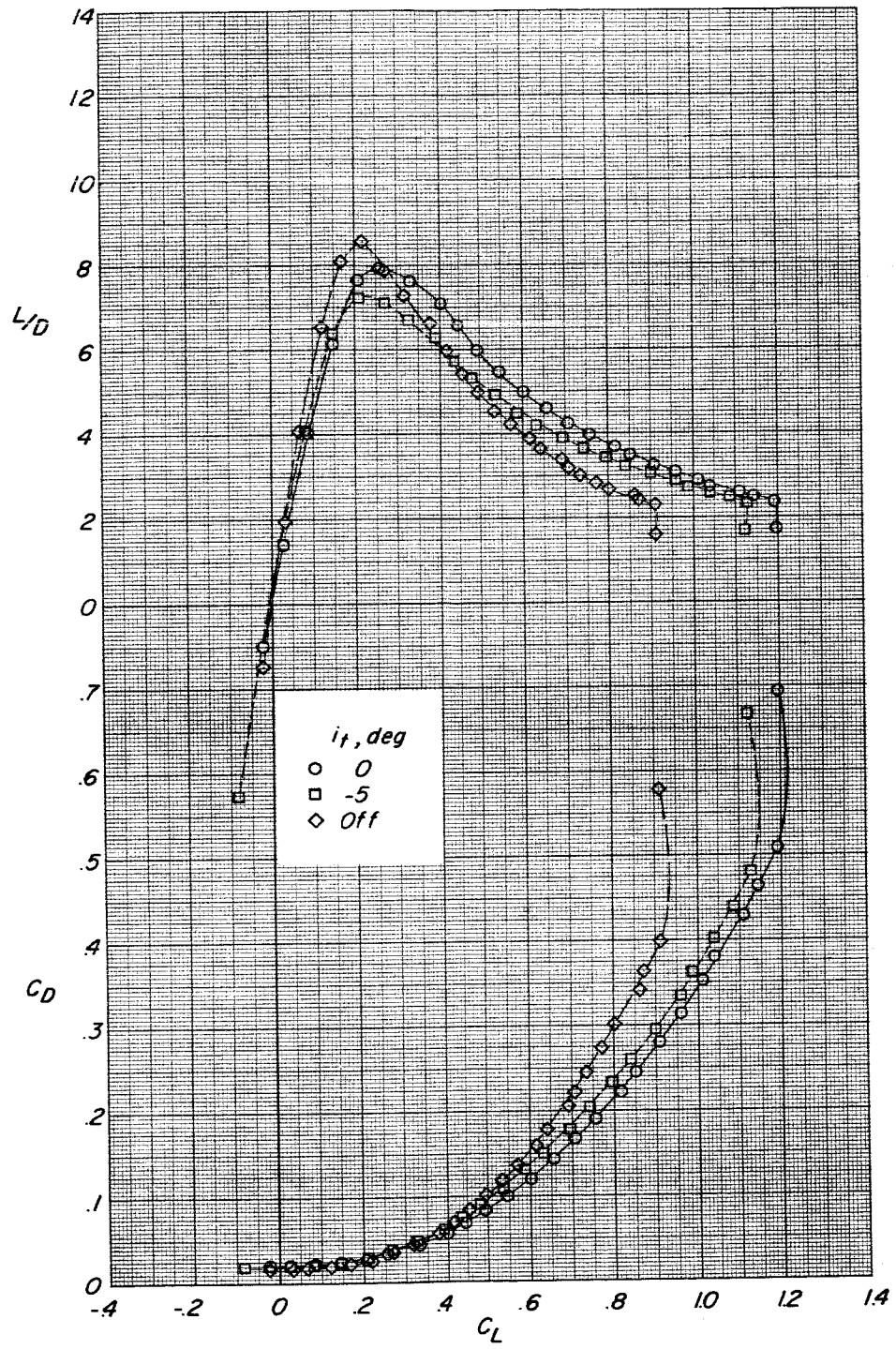

Figure 12.- Concluded.

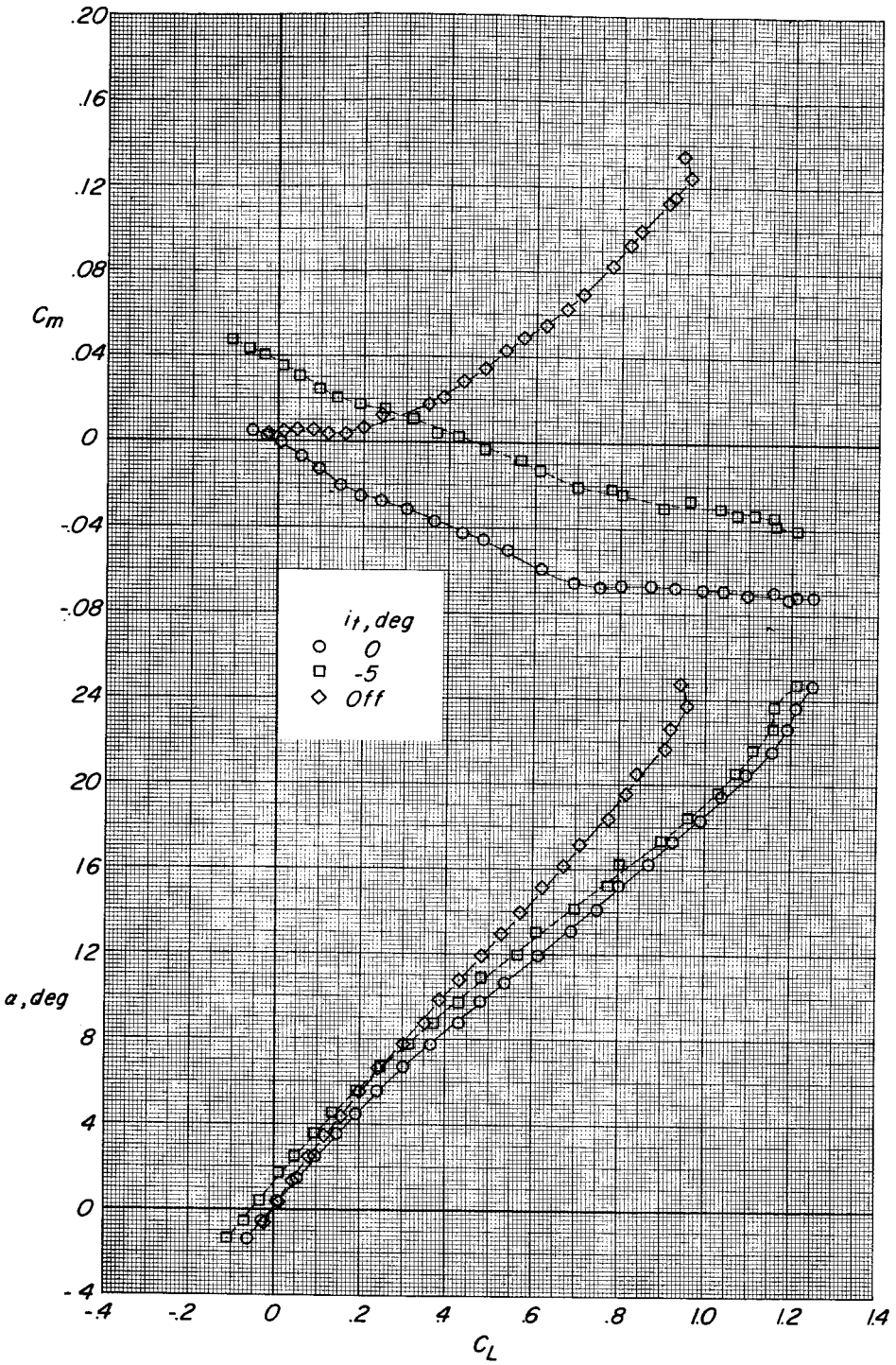

Figure 13.- Effect of horizontal-tail deflection on subsonic longitudinal aerodynamic characteristics of configuration IV with $\Lambda = 71.50^\circ$. $\Gamma_t = 0^\circ$; M = 0.23.

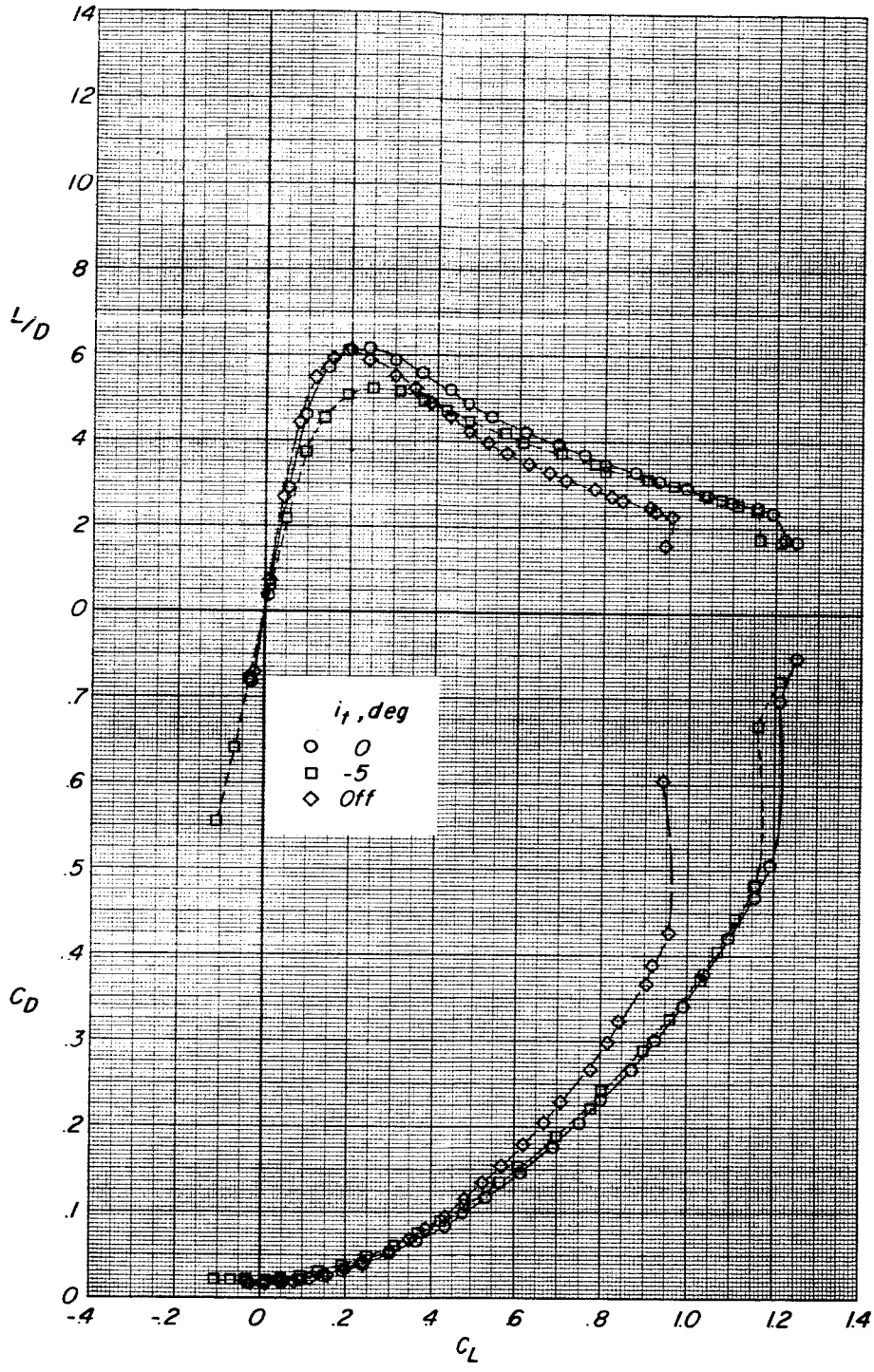

Figure 13.- Concluded.

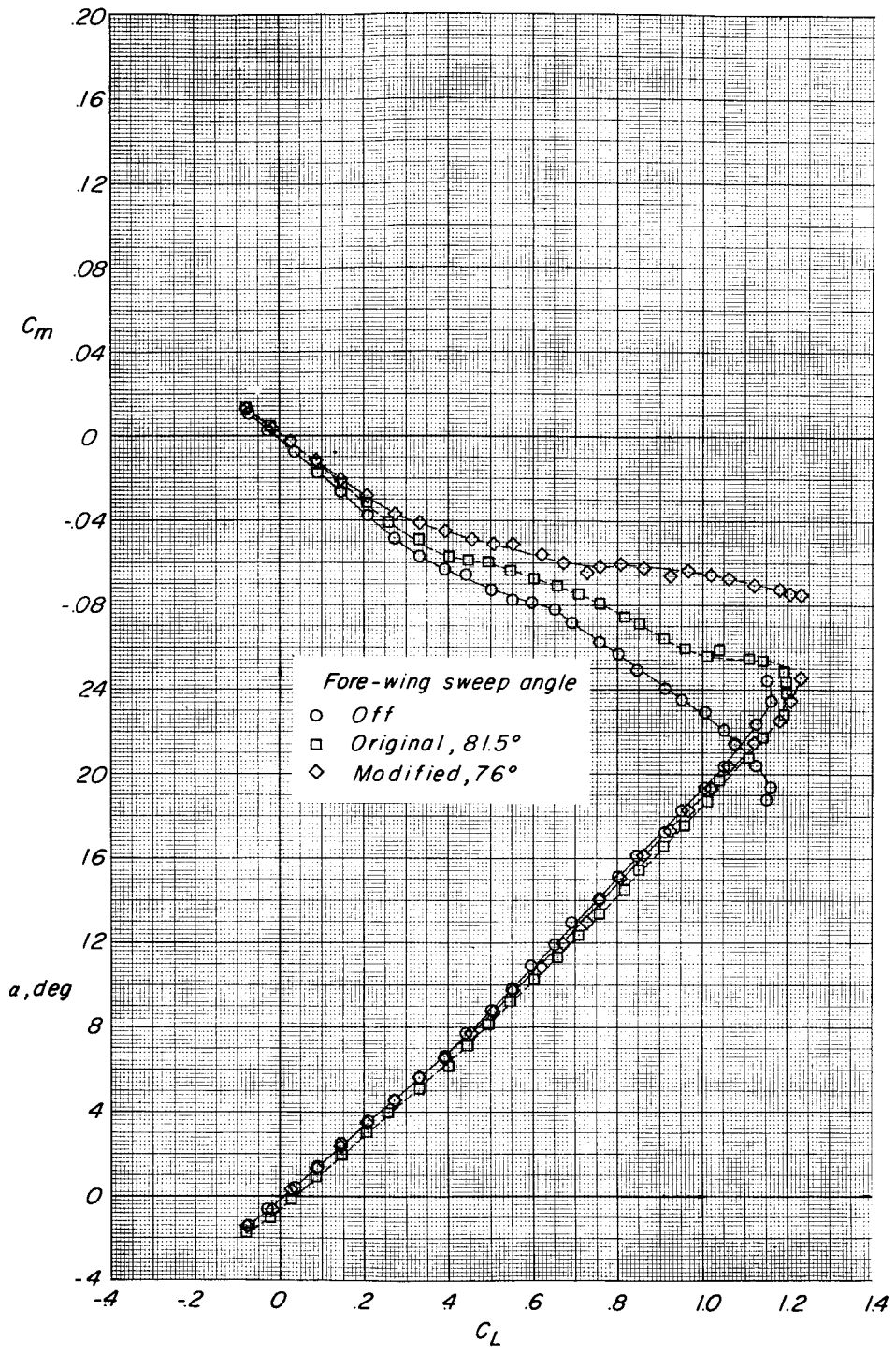

Figure 14.- Effect of fore-wing sweep angle on subsonic longitudinal aerodynamic characteristics of configuration IV with $\Lambda = 48.25^{\circ}$. $\Gamma_t = 0^{\circ}$; M = 0.23.

[redacted]

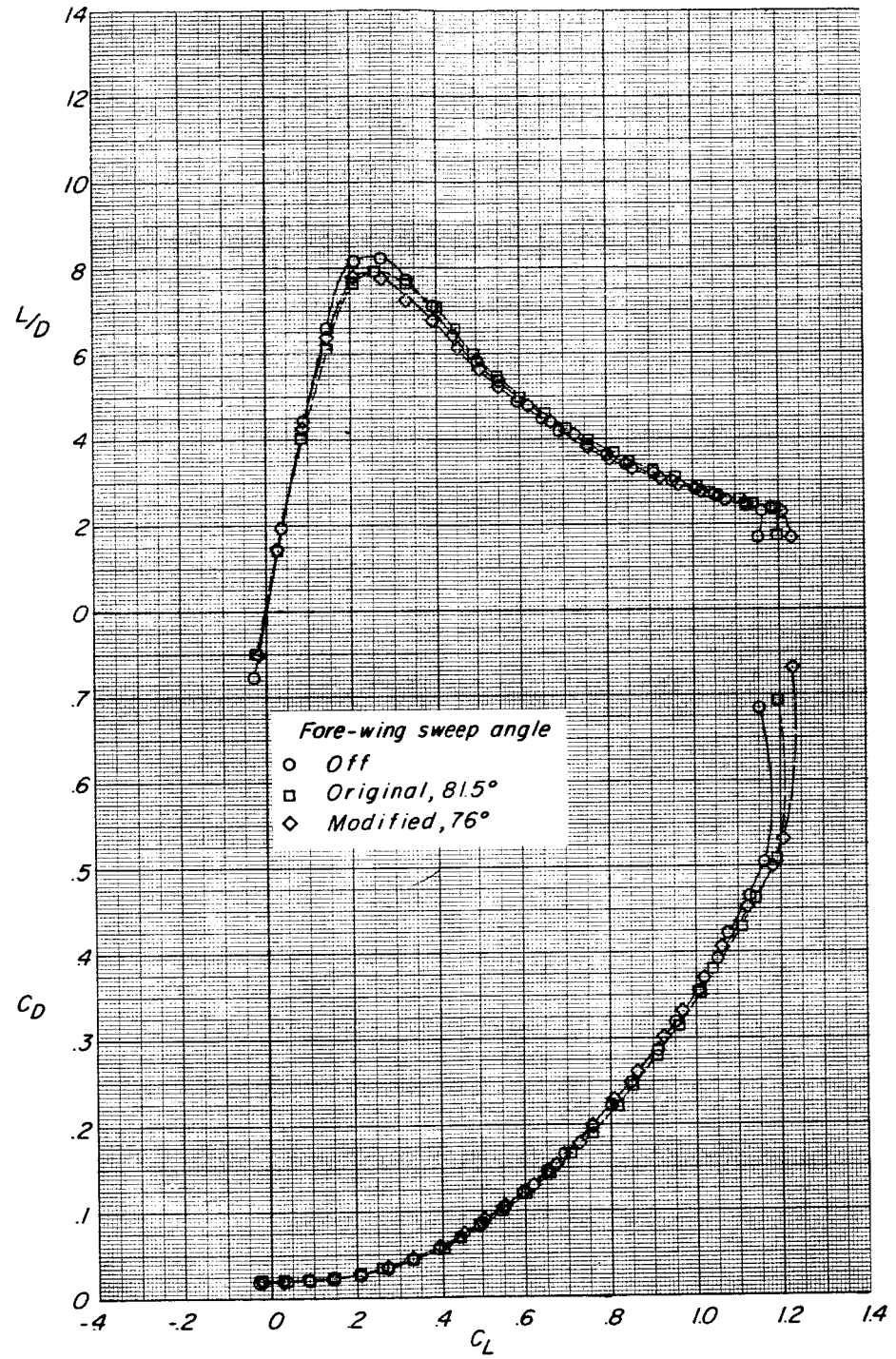

Figure 14.- Concluded.

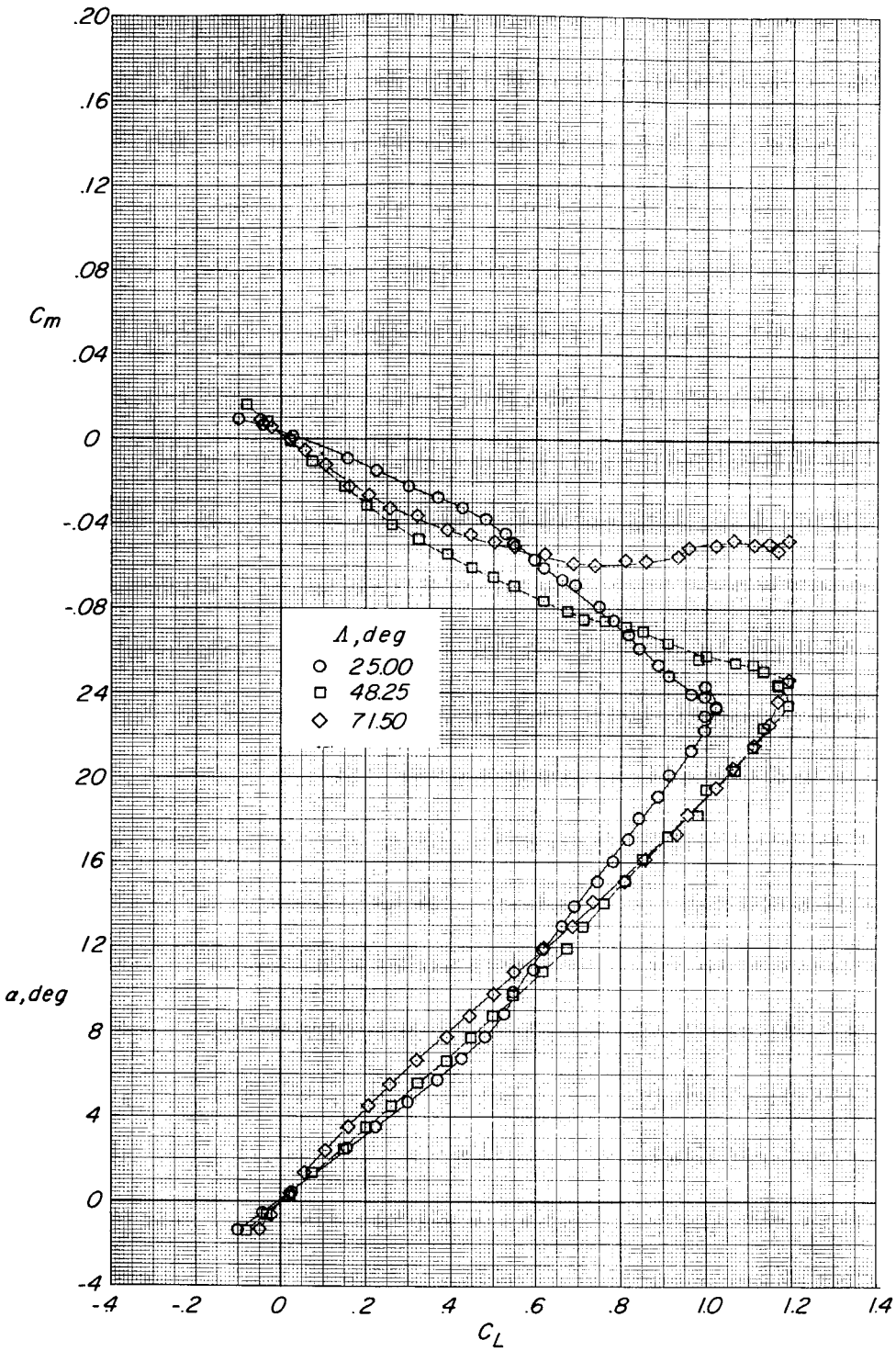

Figure 15.- Effect of wing sweep angle on subsonic longitudinal aerodynamic characteristics of configuration IV with $\Gamma_t = -20^\circ$. $i_t = 0^\circ$; M = 0.23.

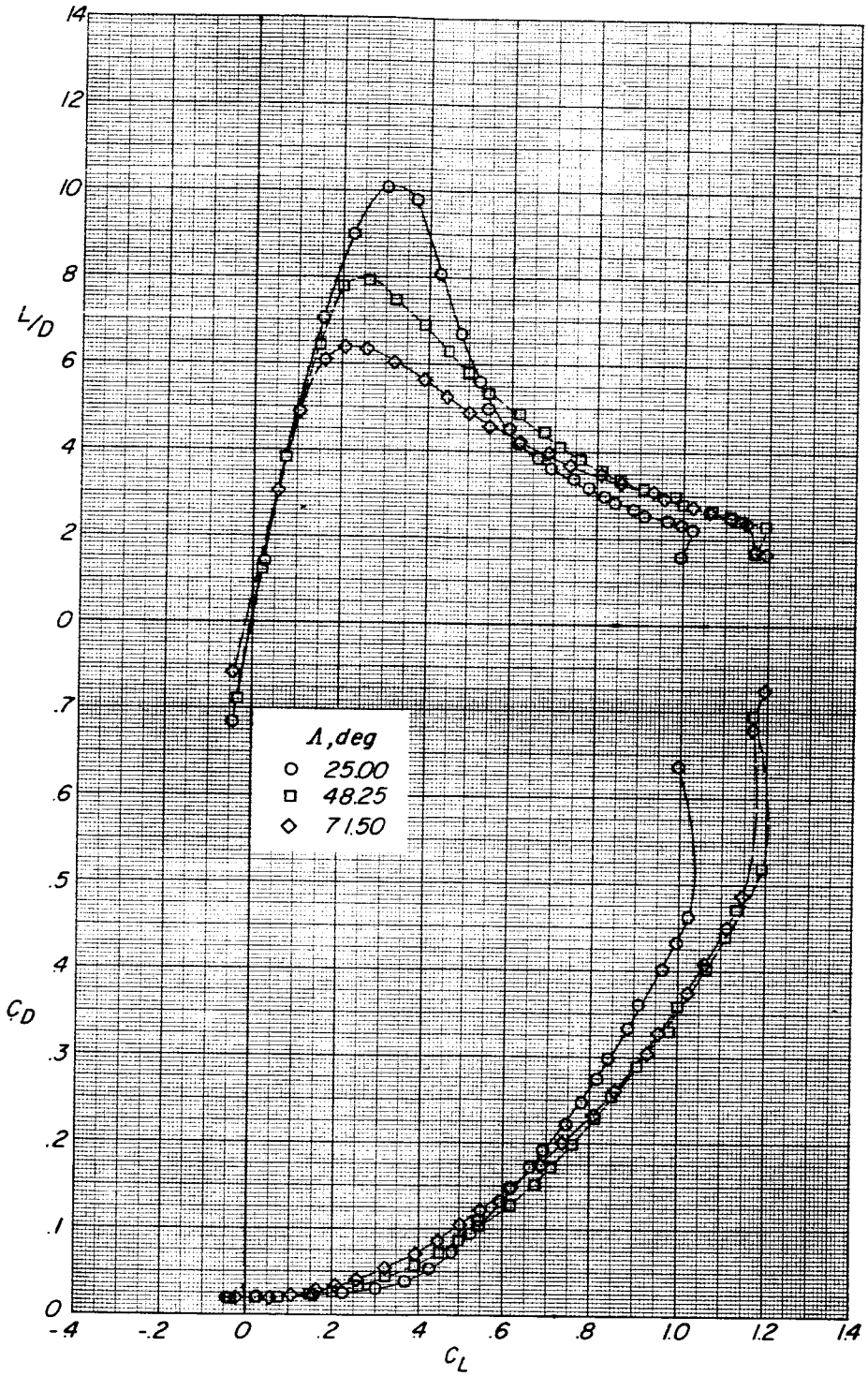

Figure 15.- Concluded.

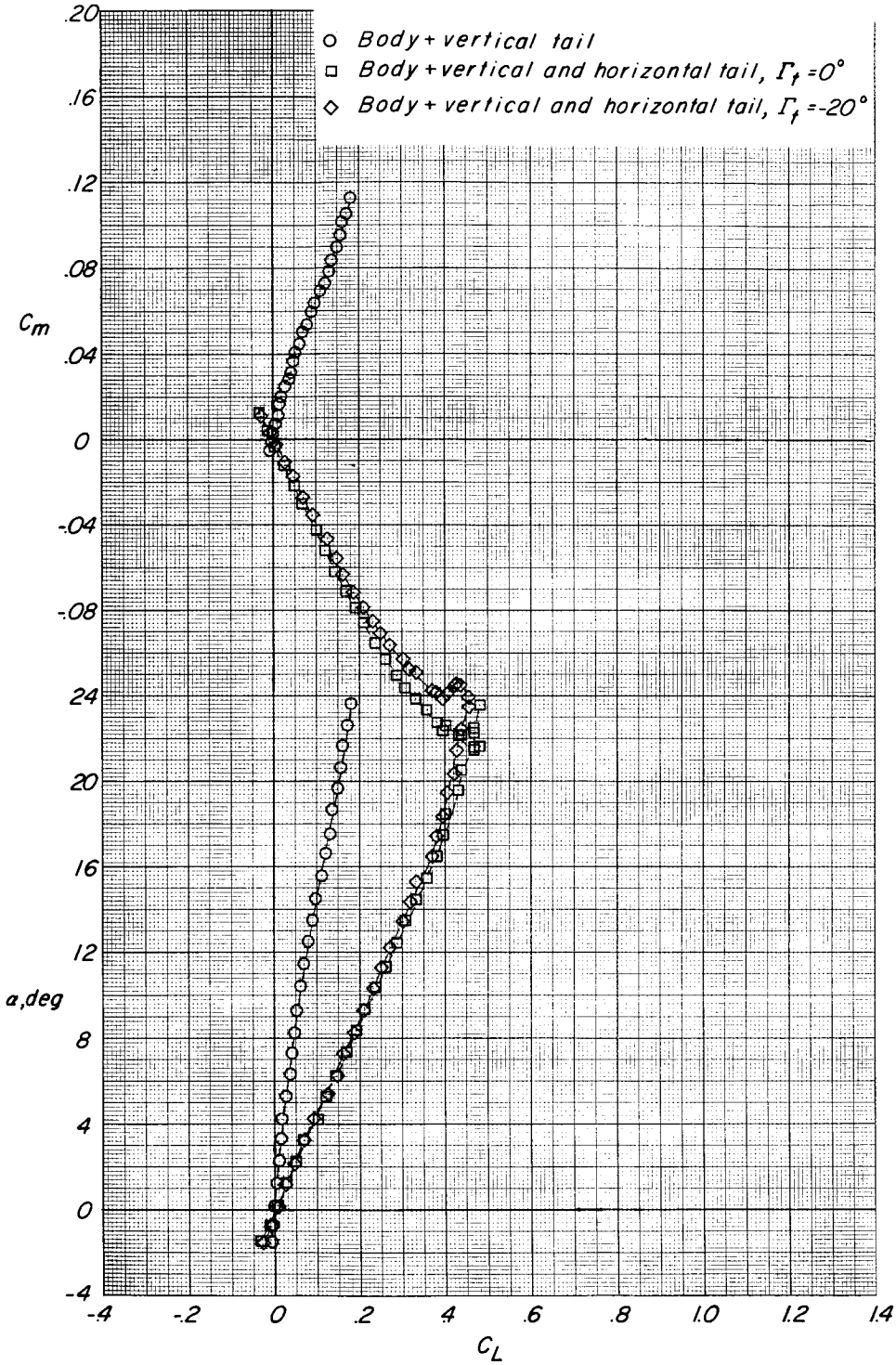

Figure 16.- Subsonic longitudinal aerodynamic characteristics of body and tail components of configurations III and IV. M = 0.23.

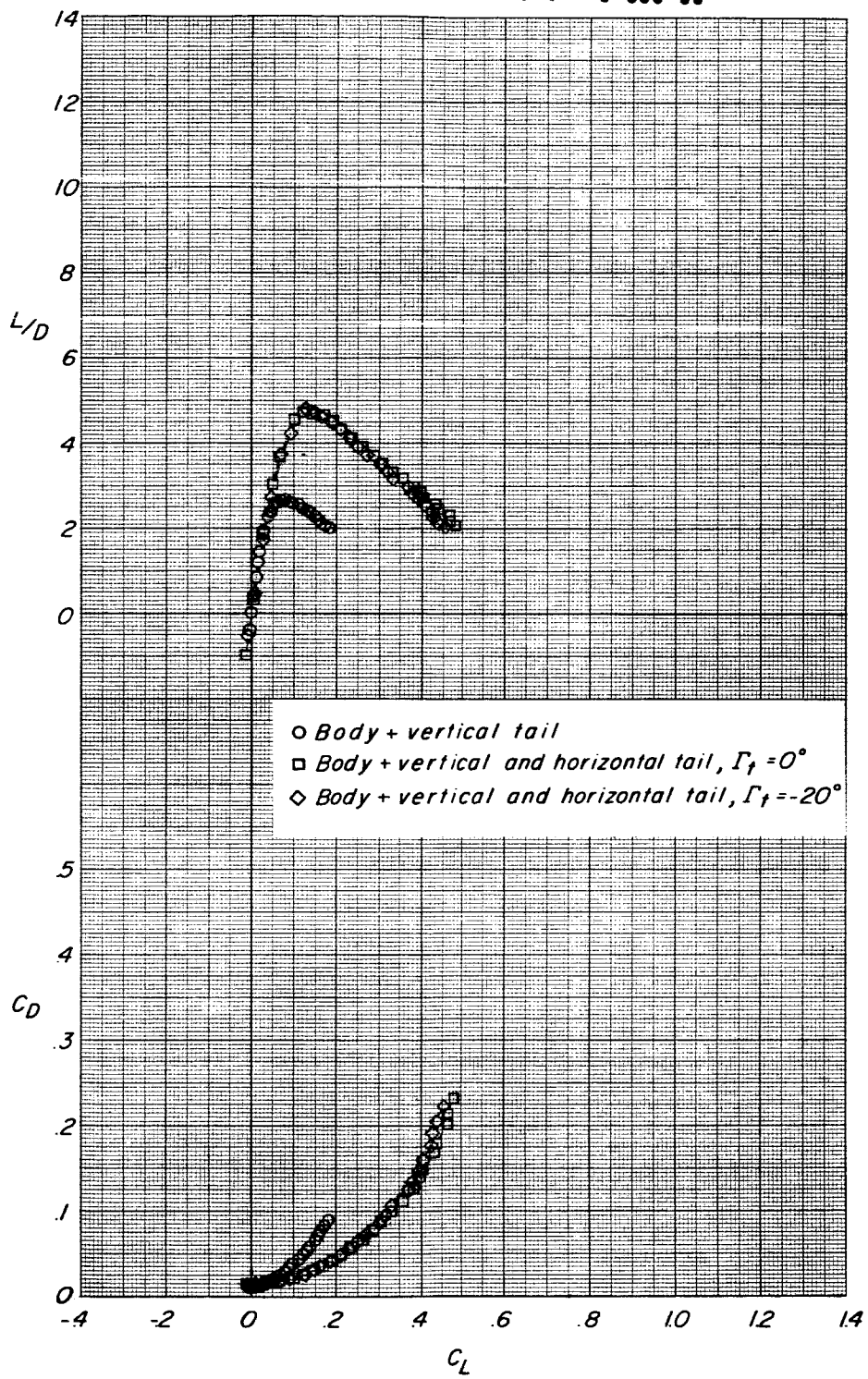

Figure 16.- Concluded.

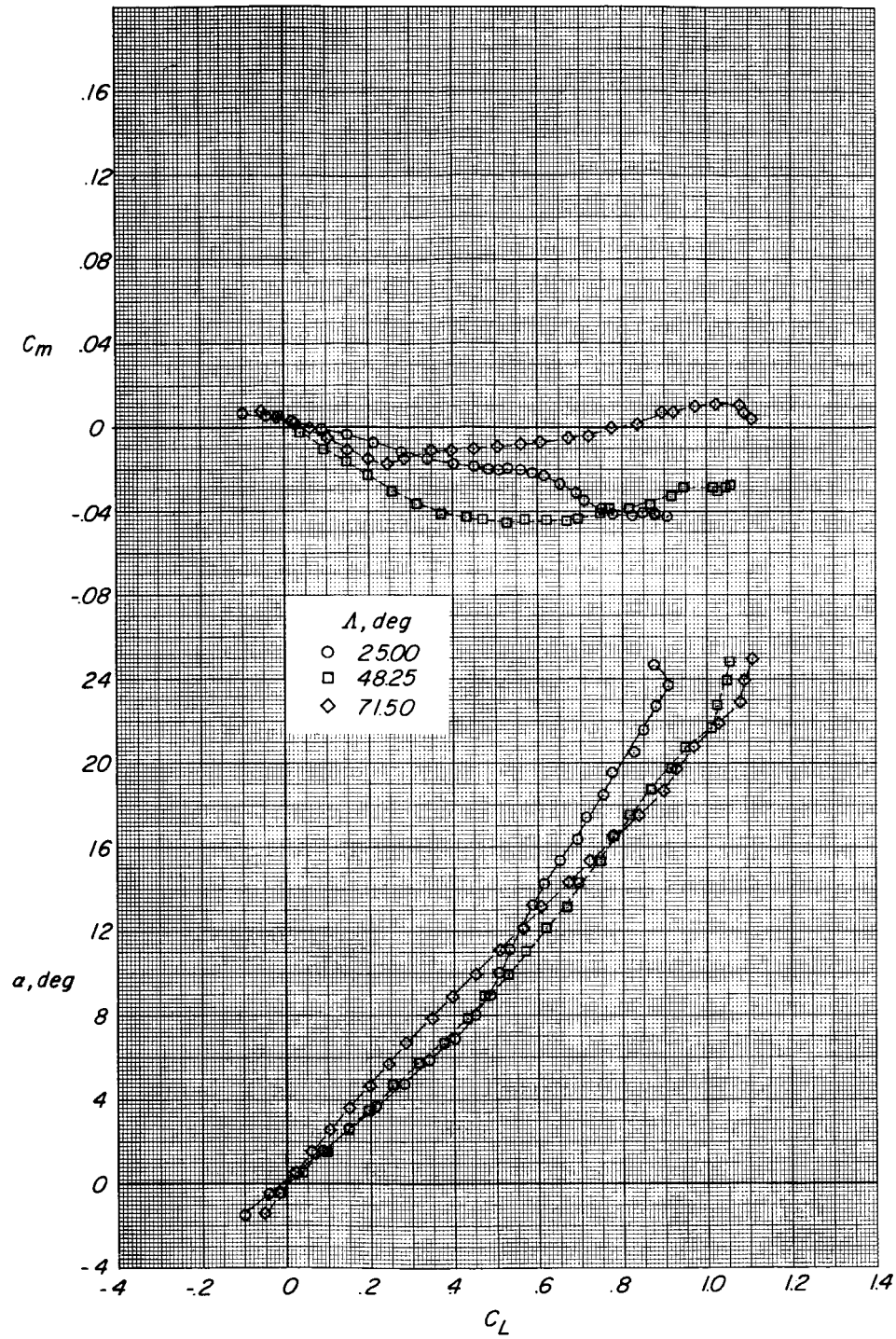

Figure 17.- Effect of wing sweep angle on subsonic longitudinal aerodynamic characteristics of configuration IV-A. $\Gamma_t = 0^\circ$; $i_t = 0^\circ$; M = 0.23.

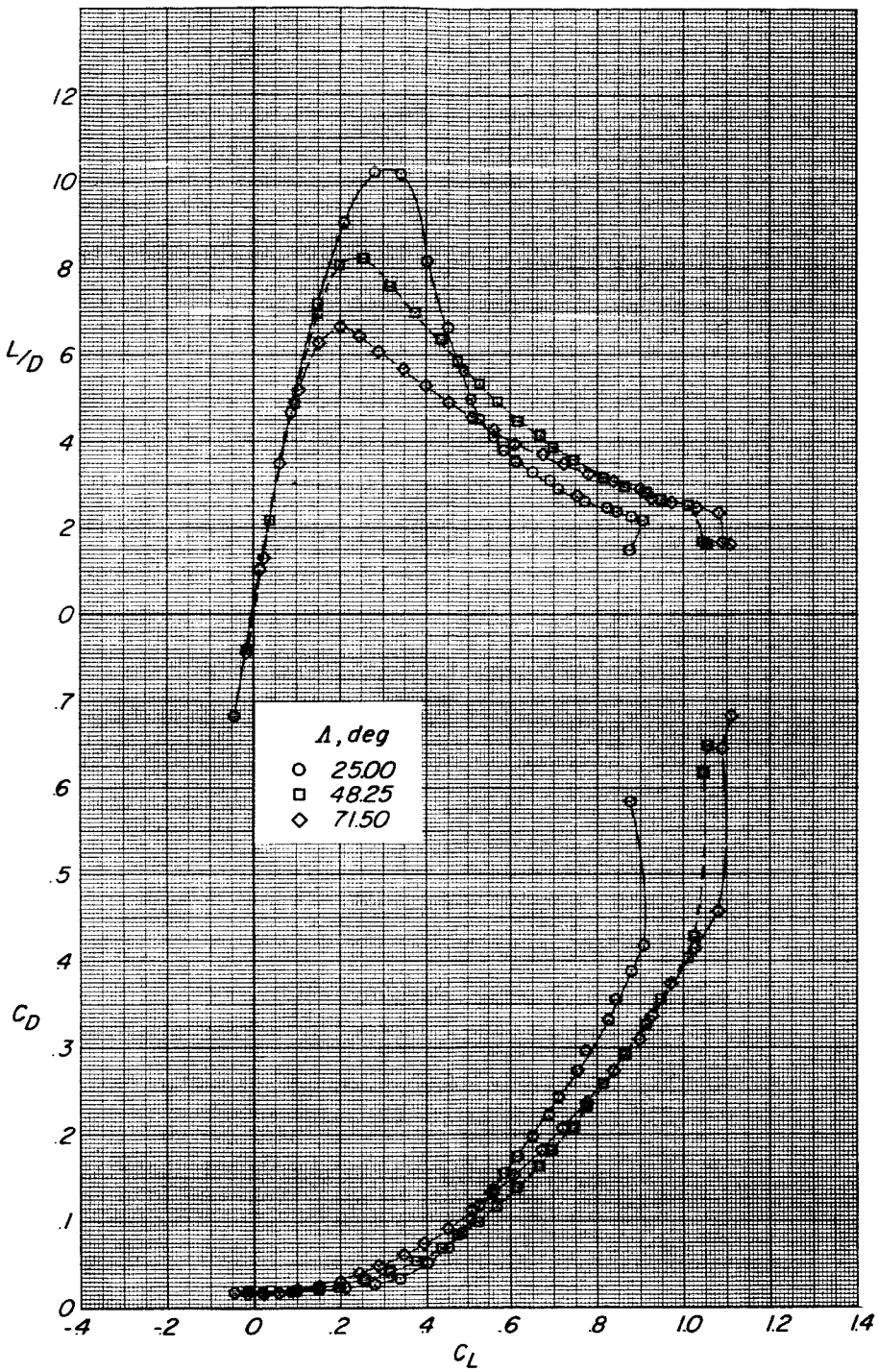

Figure 17.- Concluded.

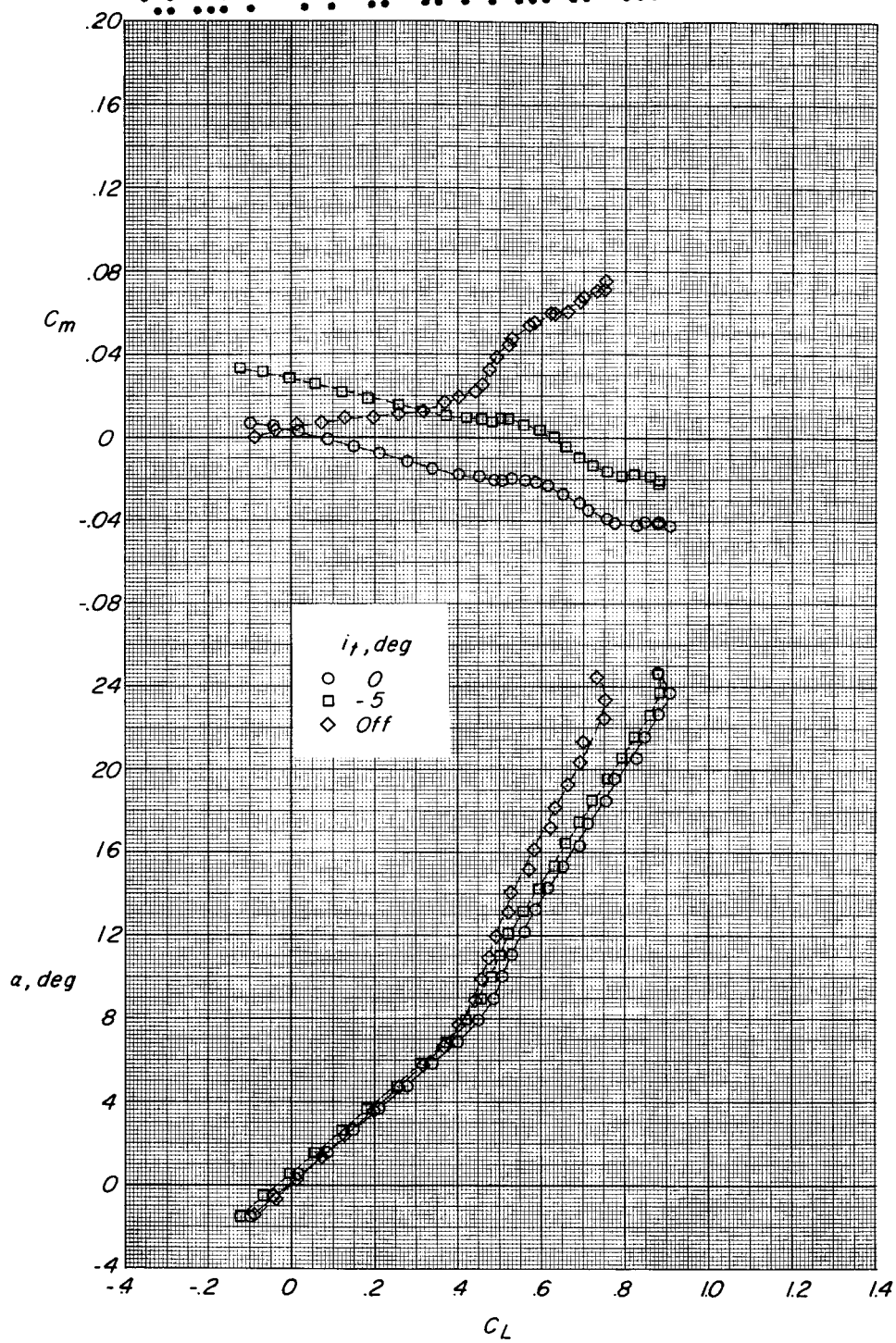

Figure 18.- Effect of horizontal-tail deflection on subsonic longitudinal aerodynamic characteristics of configuration IV-A with $\Lambda = 25.00^\circ$. $\Gamma_t = 0^\circ$; M = 0.23.

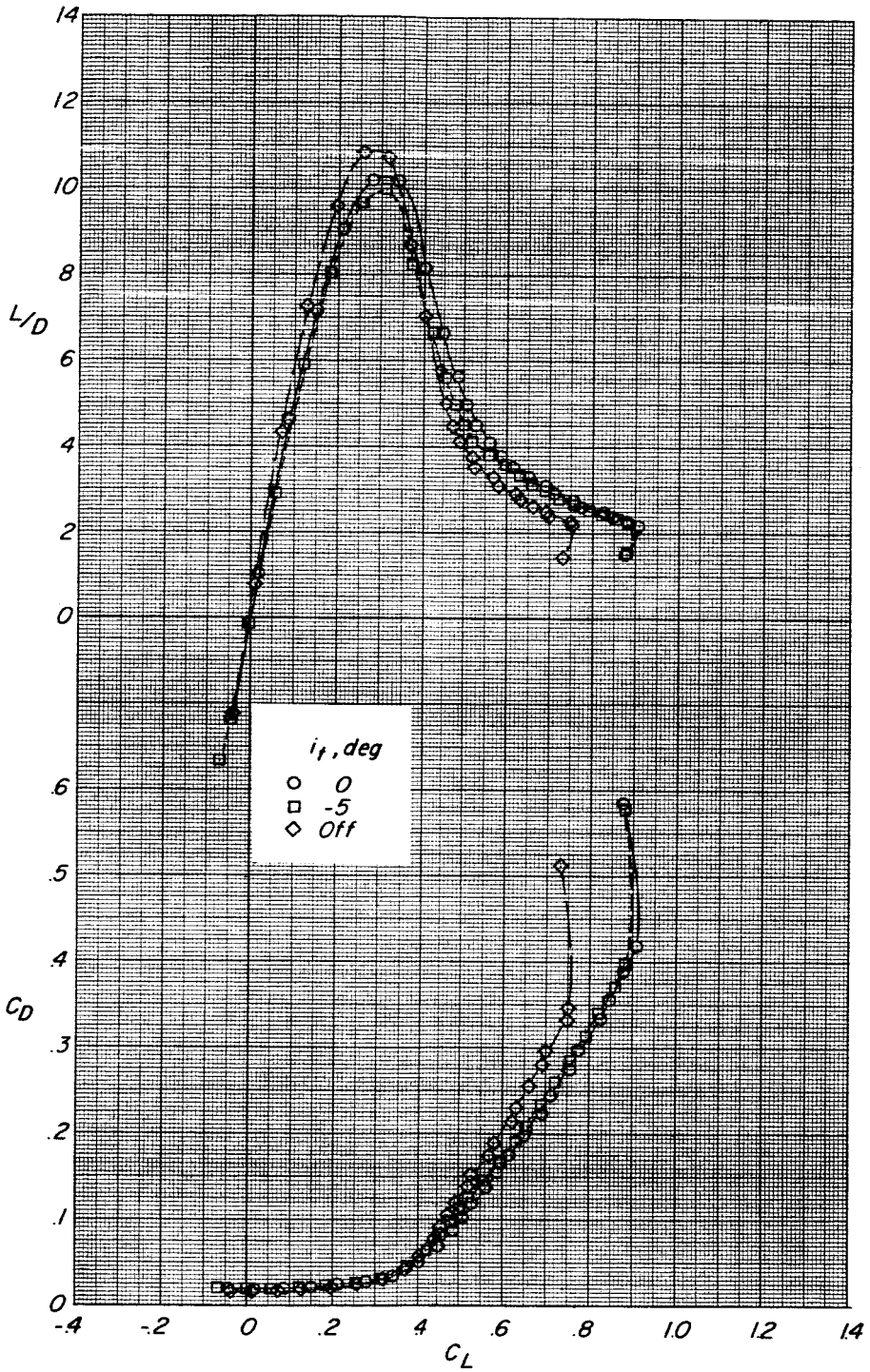

Figure 18.- Concluded.

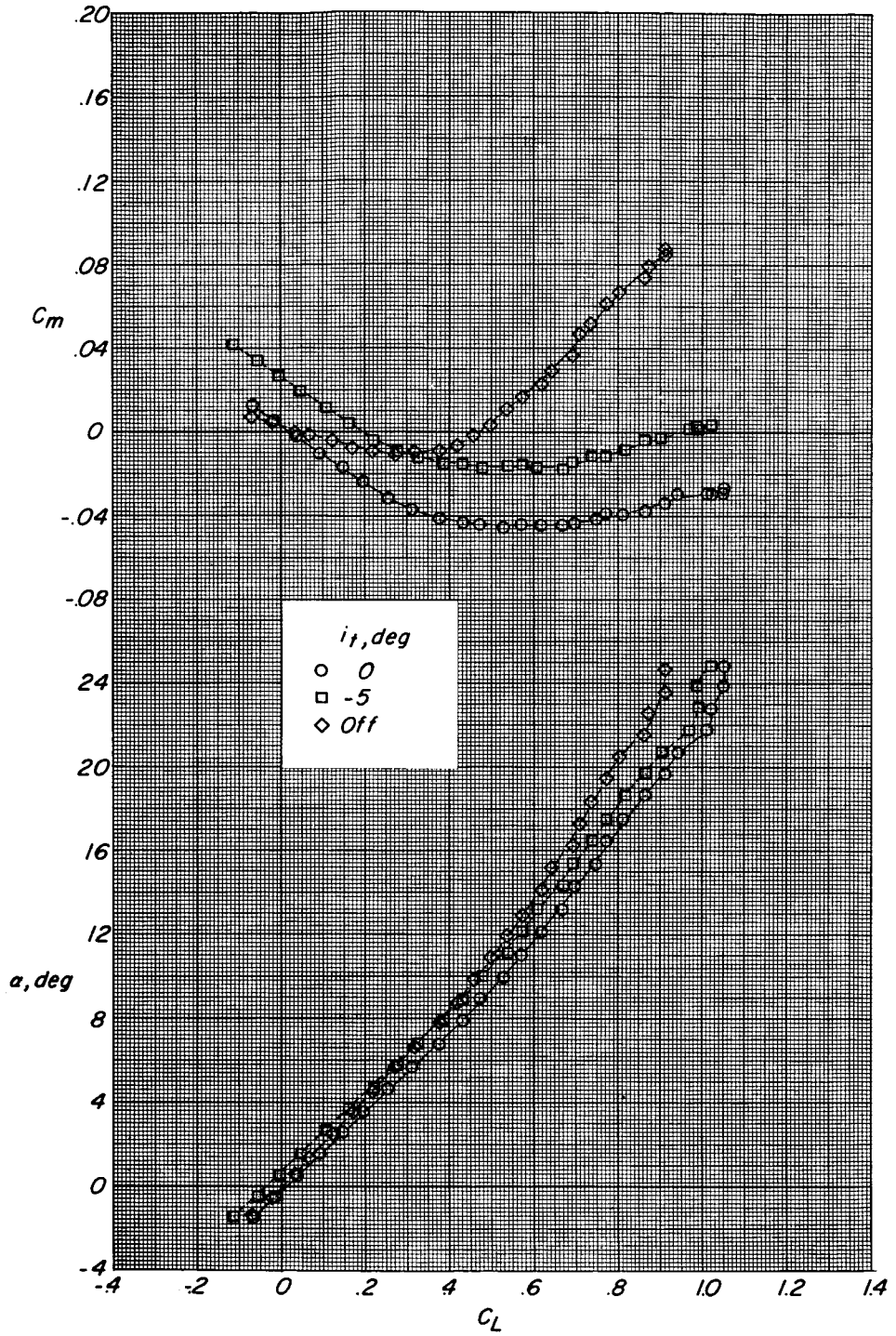

Figure 19.- Effect of horizontal-tail deflection on subsonic longitudinal aerodynamic characteristics of configuration IV-A with $\Lambda = 48.25^\circ$. $\Gamma_t = 0^\circ$; M = 0.23.

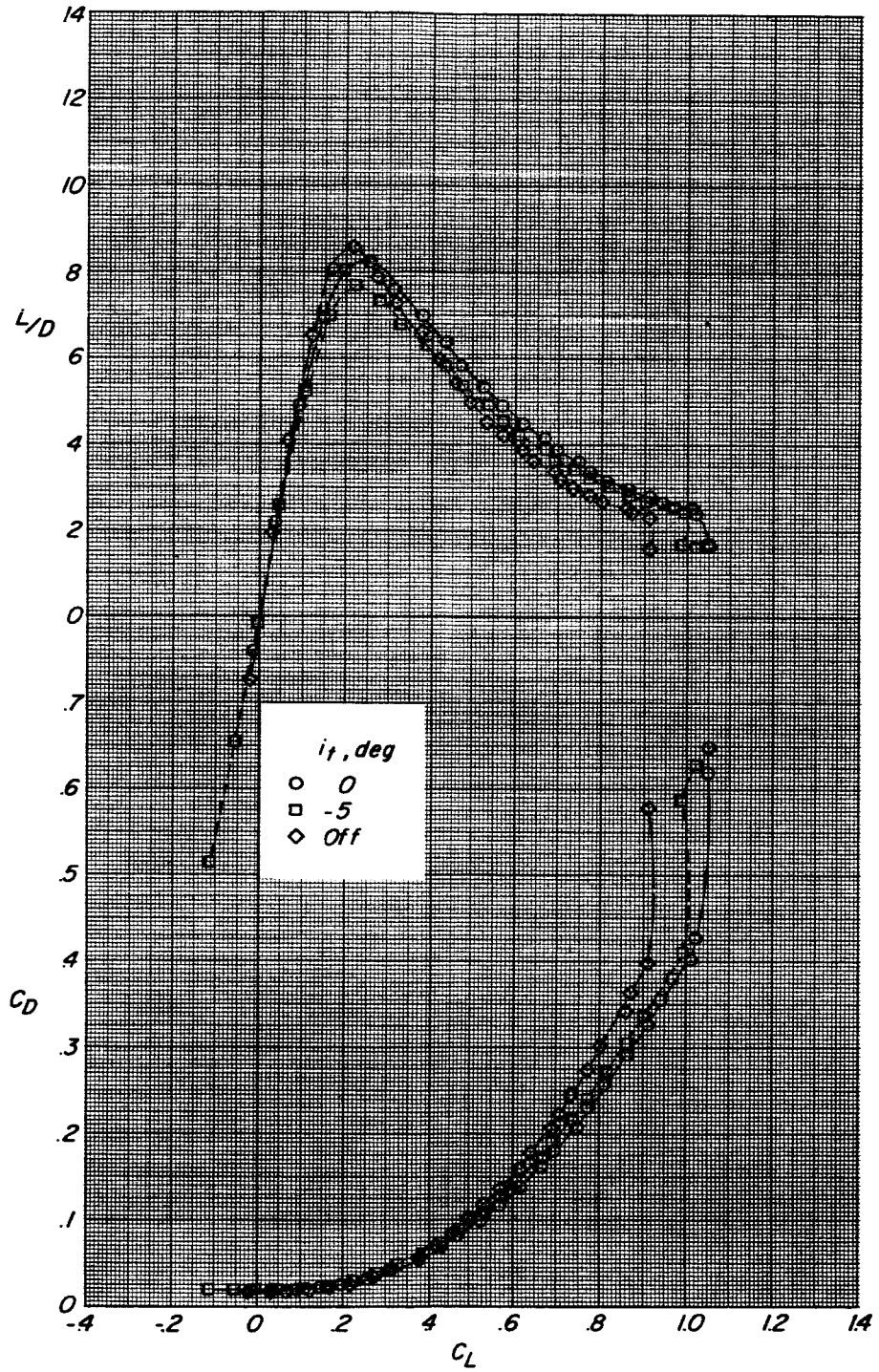

Figure 19.- Concluded.

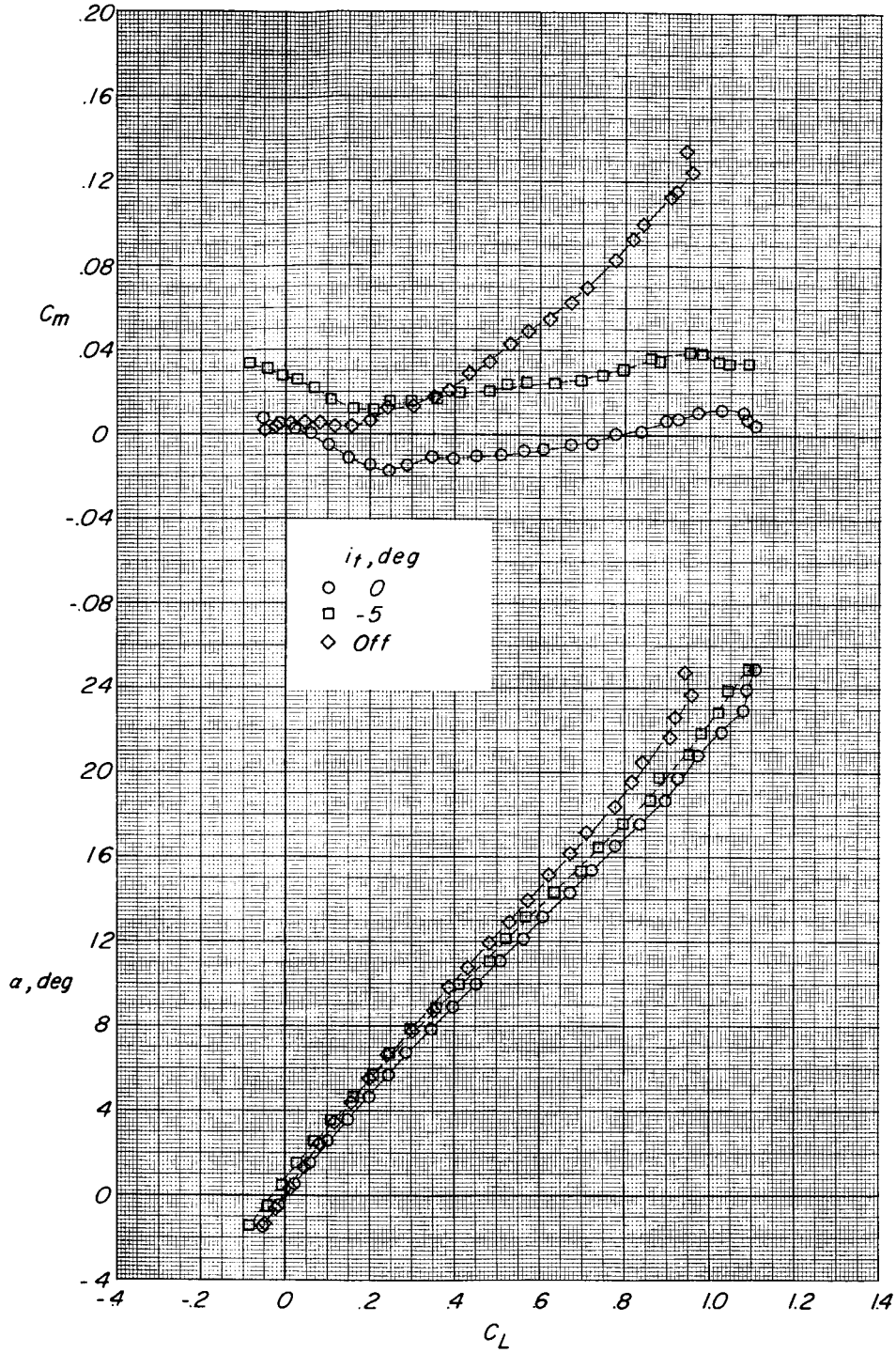

Figure 20.- Effect of horizontal-tail deflection on subsonic longitudinal aerodynamic characteristics of configuration IV-A with $\Lambda = 71.50^{\circ}$. $\Gamma_t = 0^{\circ}$; M = 0.23.

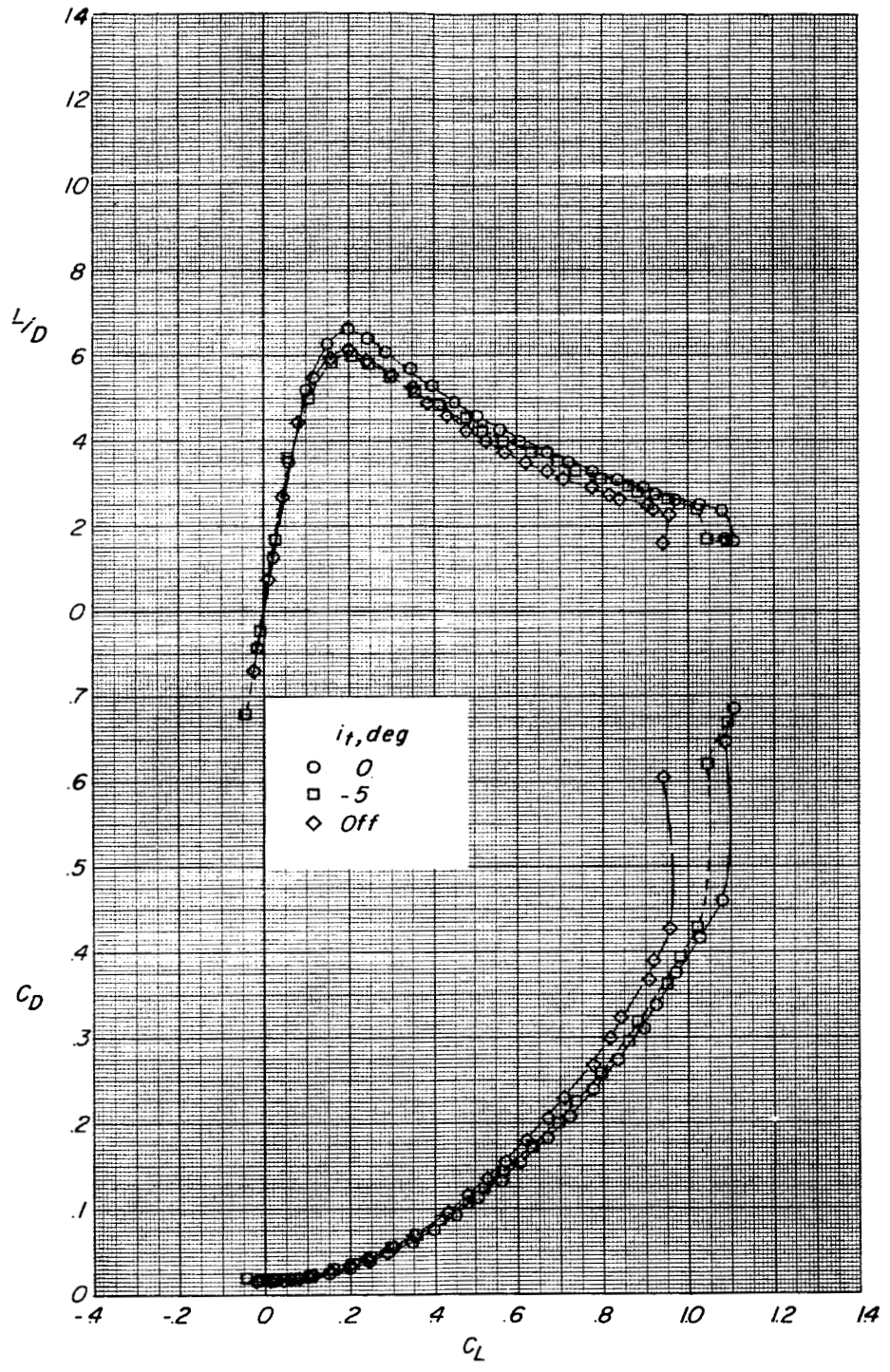

Figure 20.- Concluded.

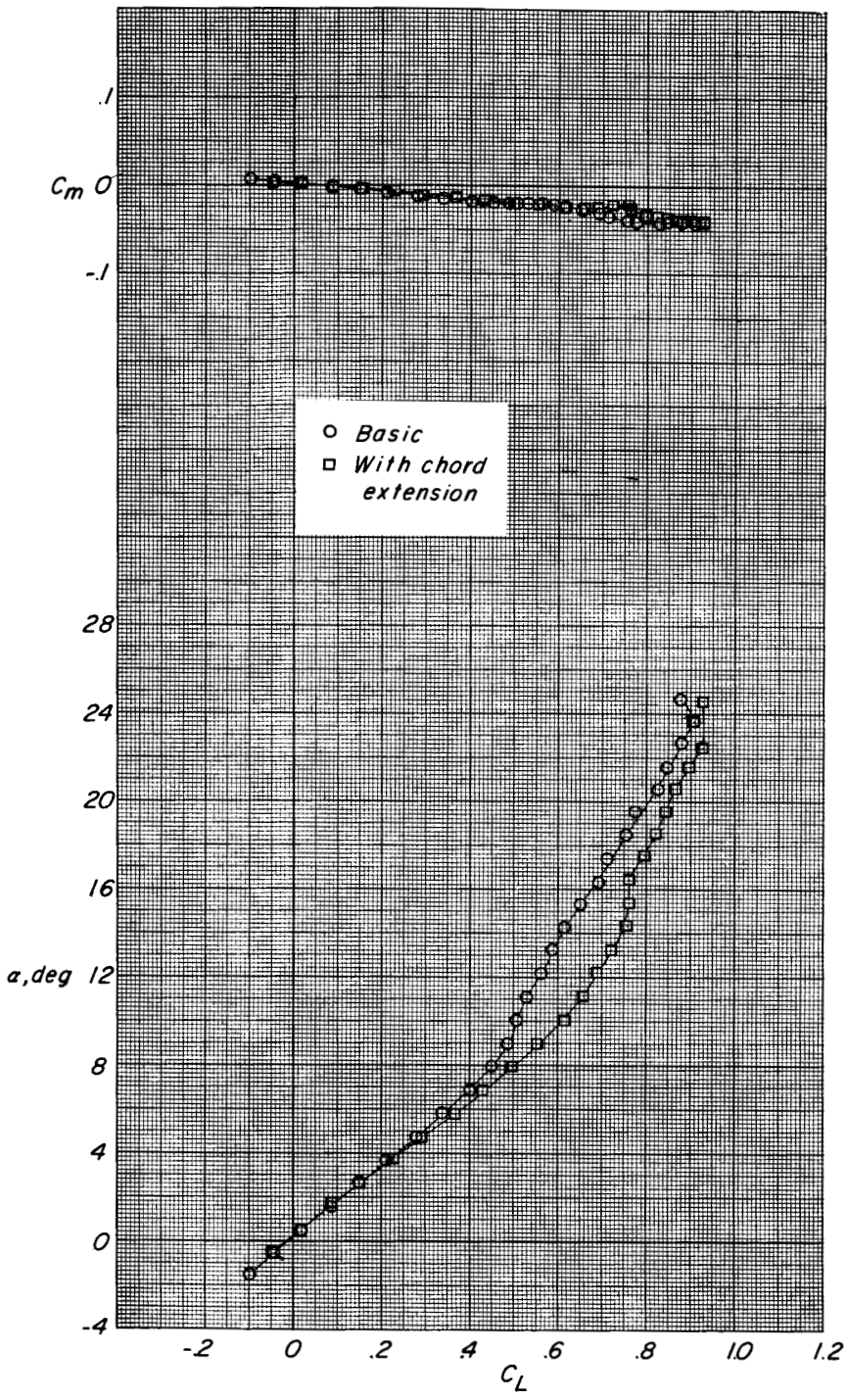

Figure 21.- Effect of a leading-edge chord extension on subsonic longitudinal aerodynamic characteristics of configuration IV-A. $\Lambda = 25.00^\circ$; $\Gamma_t = 0^\circ$; $i_t = 0^\circ$; M = 0.23.

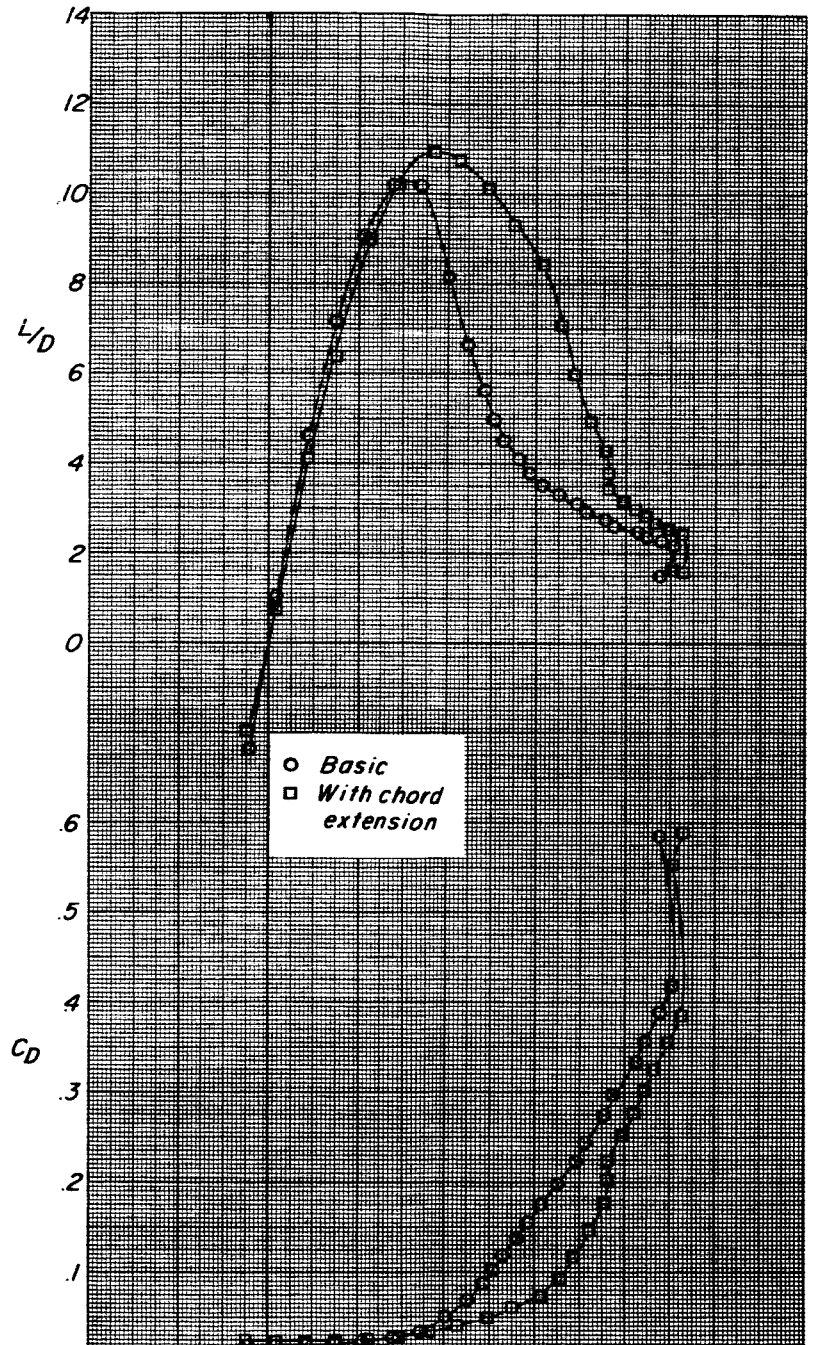

Figure 21.- Concluded.

[redacted]

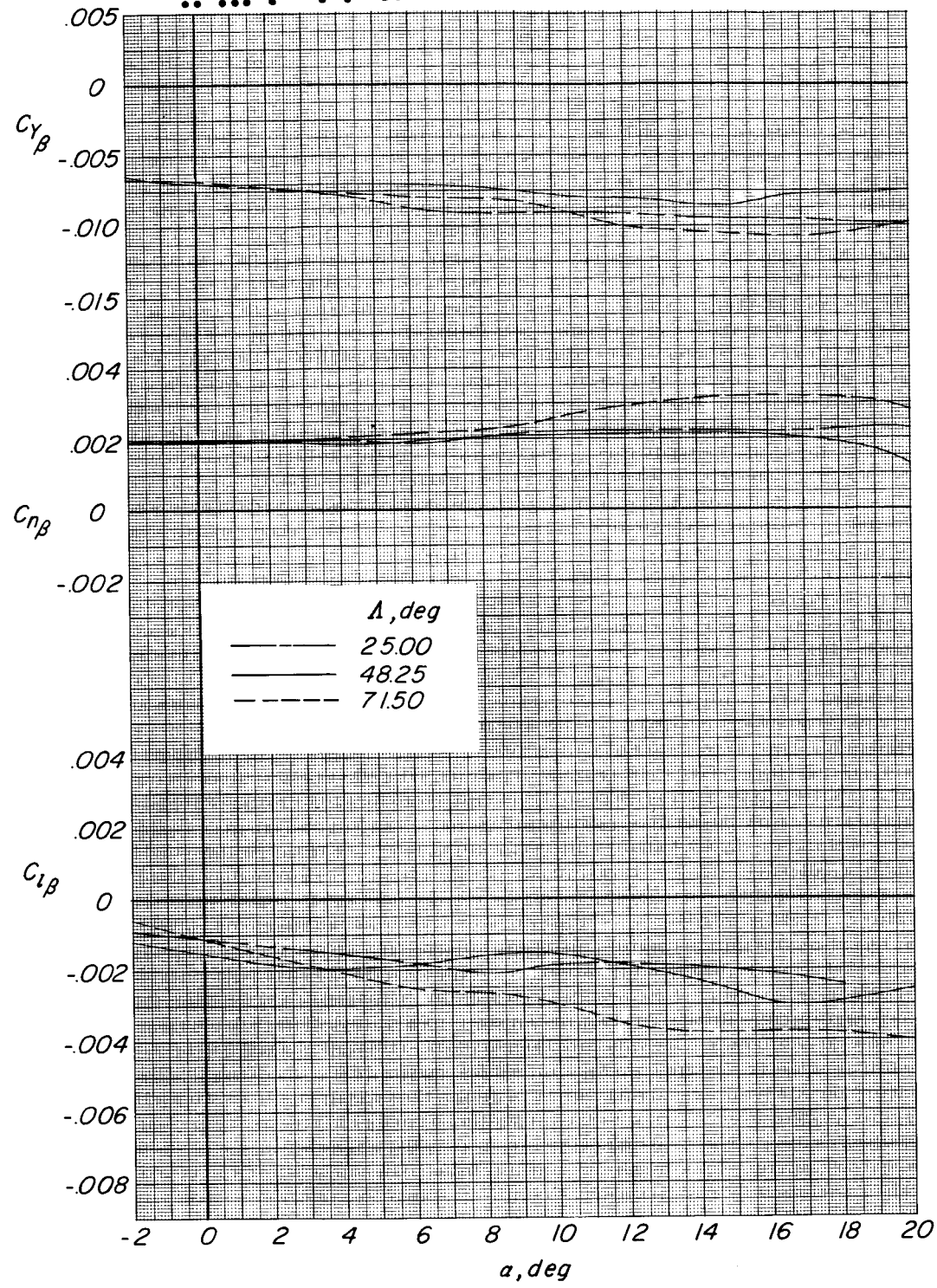

Figure 22.- Effect of wing sweep angle on subsonic lateral characteristics of configuration IV-A. $\Gamma_t = 0^\circ$; $i_t = 0^\circ$; M = 0.23.

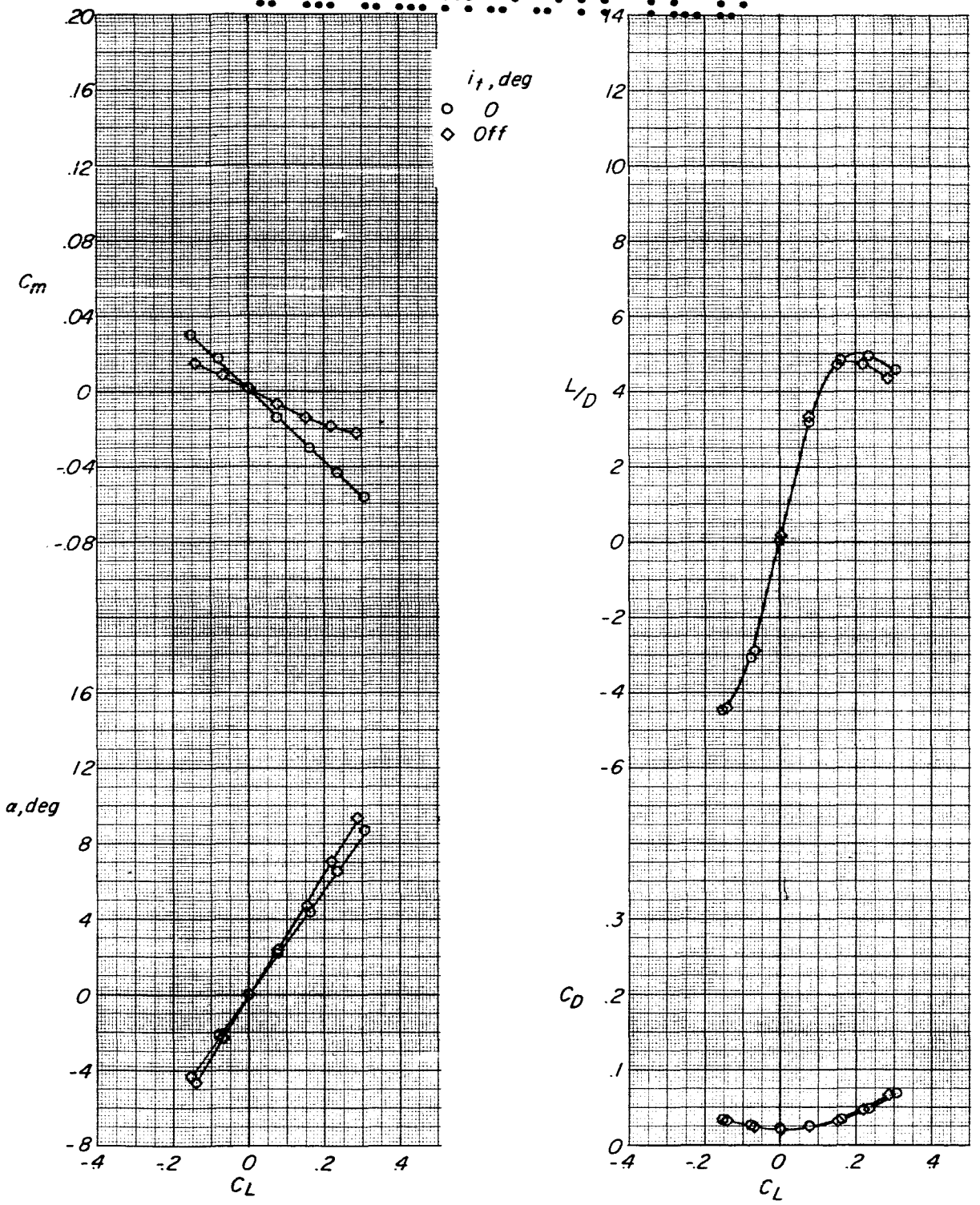

Figure 23.- Supersonic longitudinal aerodynamic characteristics of configuration IV. $\Lambda = 71.50^{\circ}$; $\Gamma_t = 0^{\circ}$; M = 2.20.

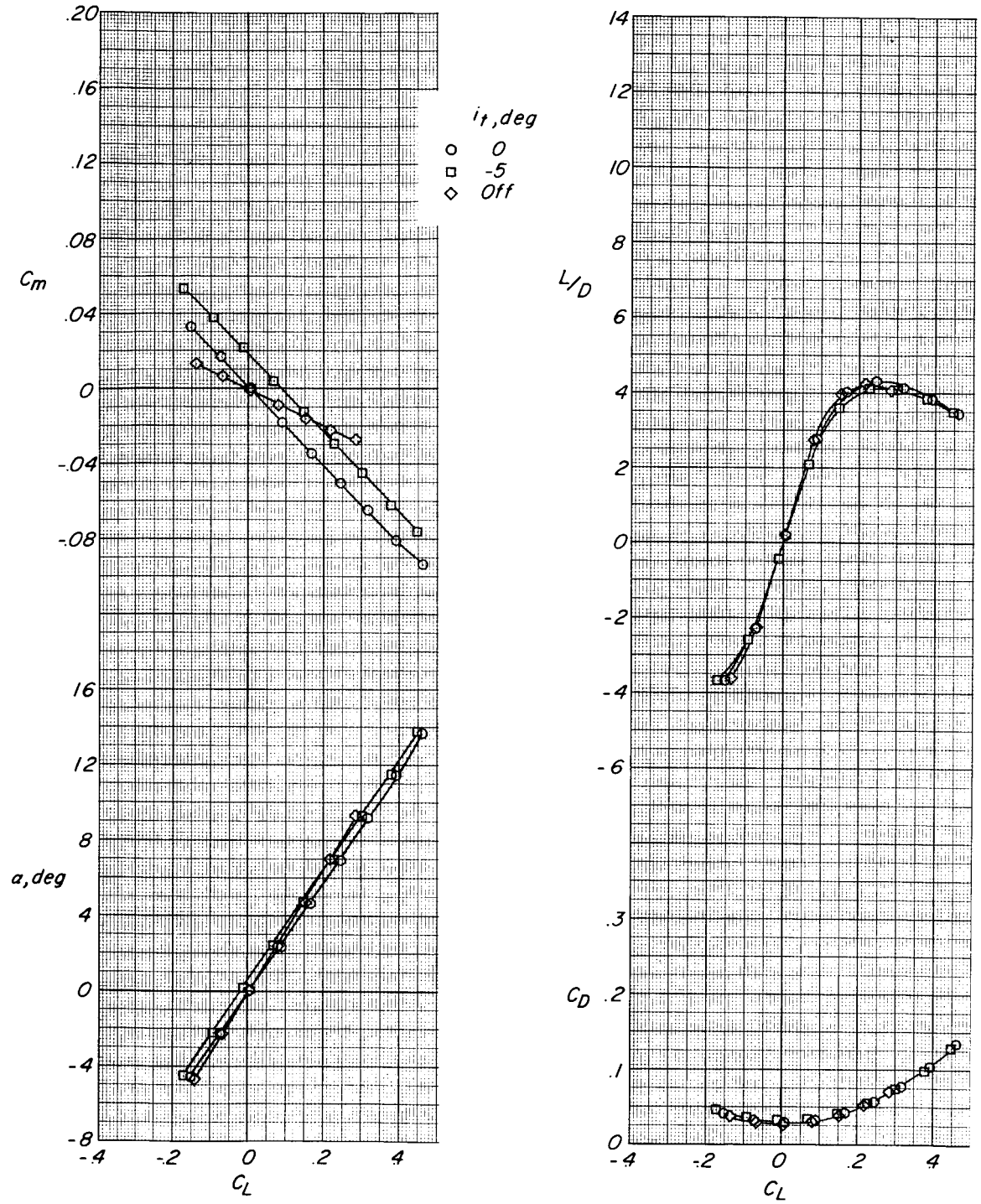

Figure 24.- Effect of horizontal-tail deflection on supersonic longitudinal aerodynamic characteristics of configuration IV-A with $\Lambda = 48.25^\circ$. $\Gamma_t = 0^\circ$; M = 2.20.

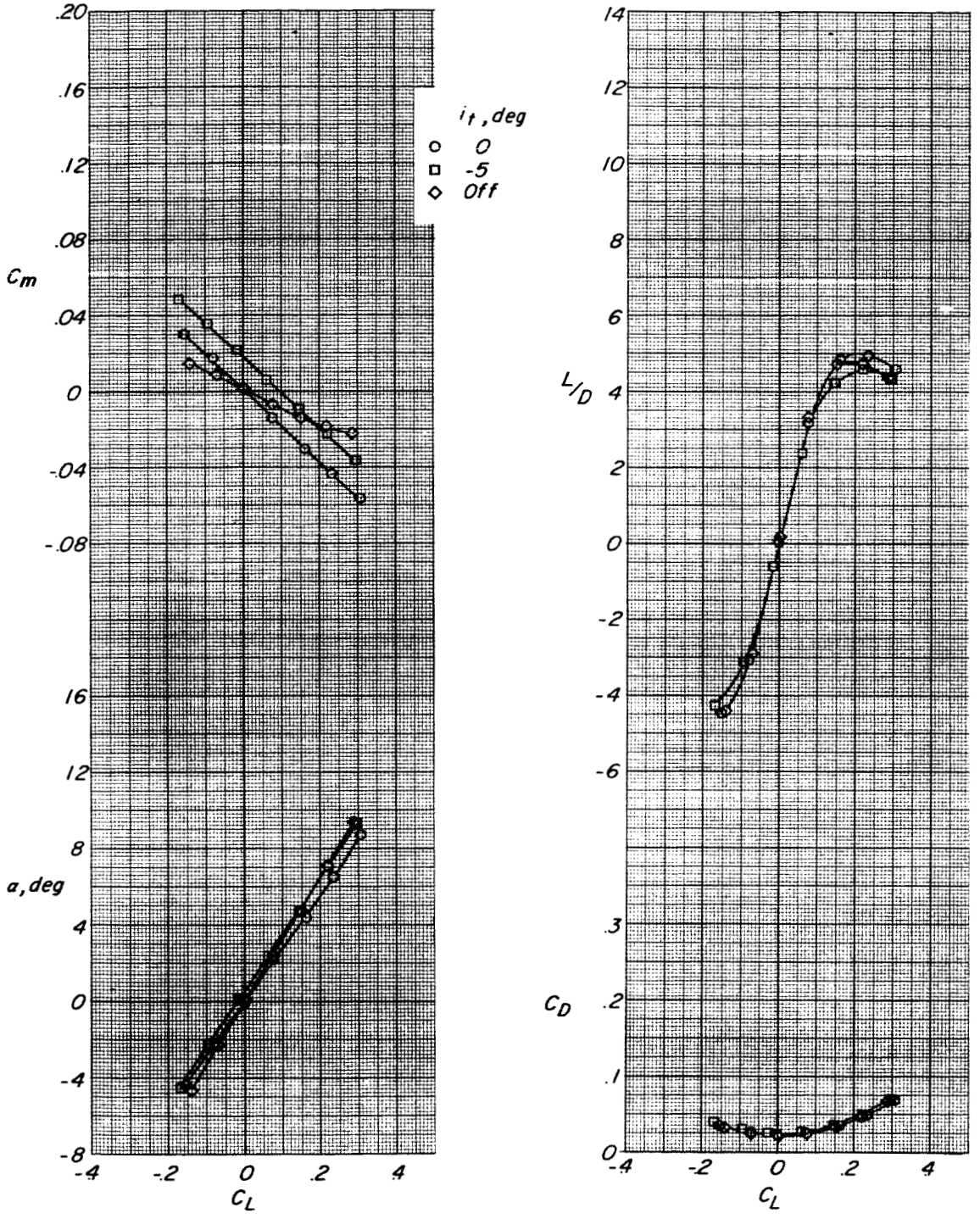

Figure 25.- Effect of horizontal-tail deflection on supersonic longitudinal aerodynamic characteristics of configuration IV-A with $\Lambda = 71.50^{\circ}$. $\Gamma_t = 0^{\circ}$; M = 2.20.

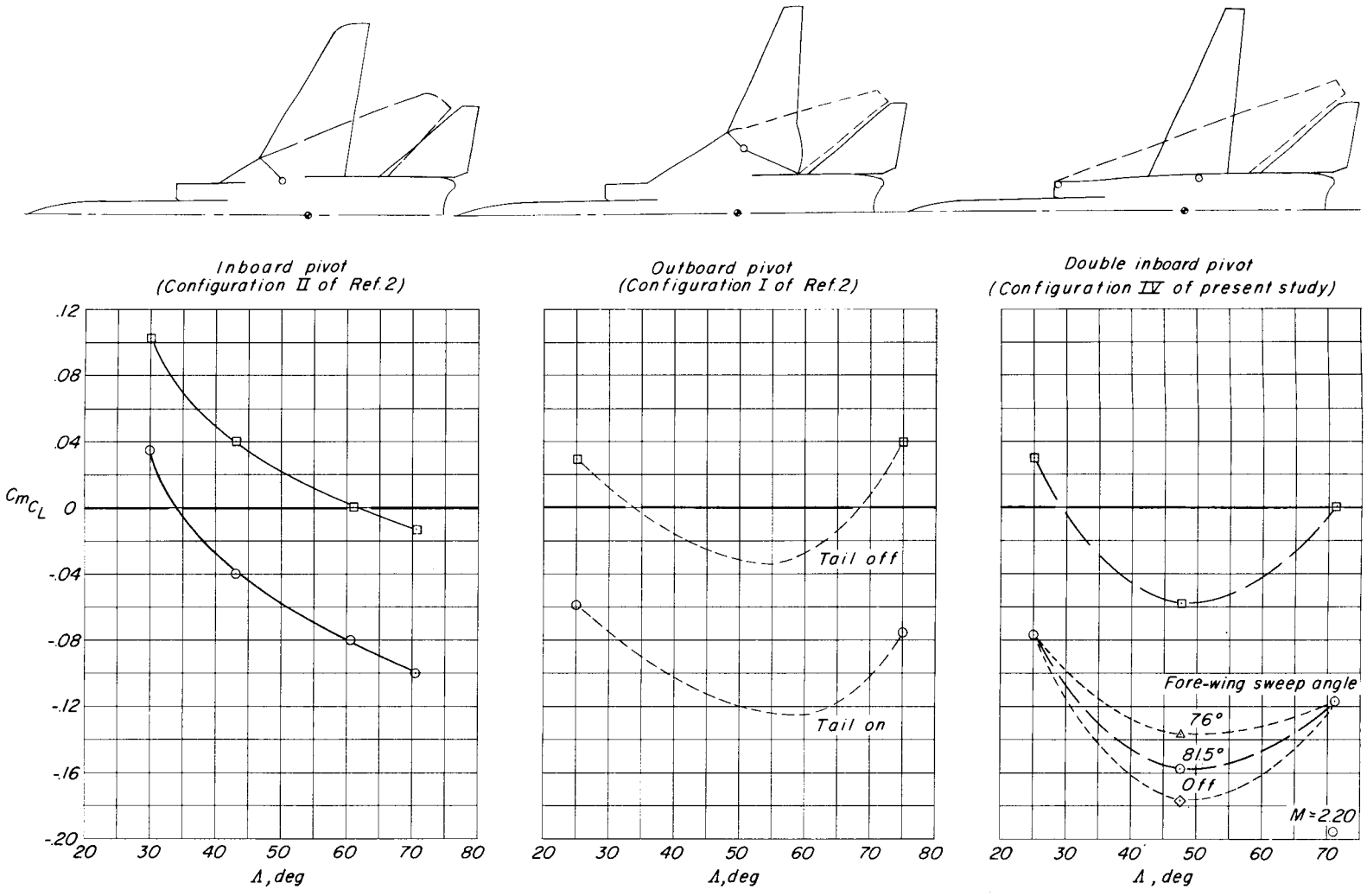

Figure 26.- Variation of $C_{m_{C_L}}$ with sweep for several configurations. $M \approx 0.23$ except where otherwise noted.

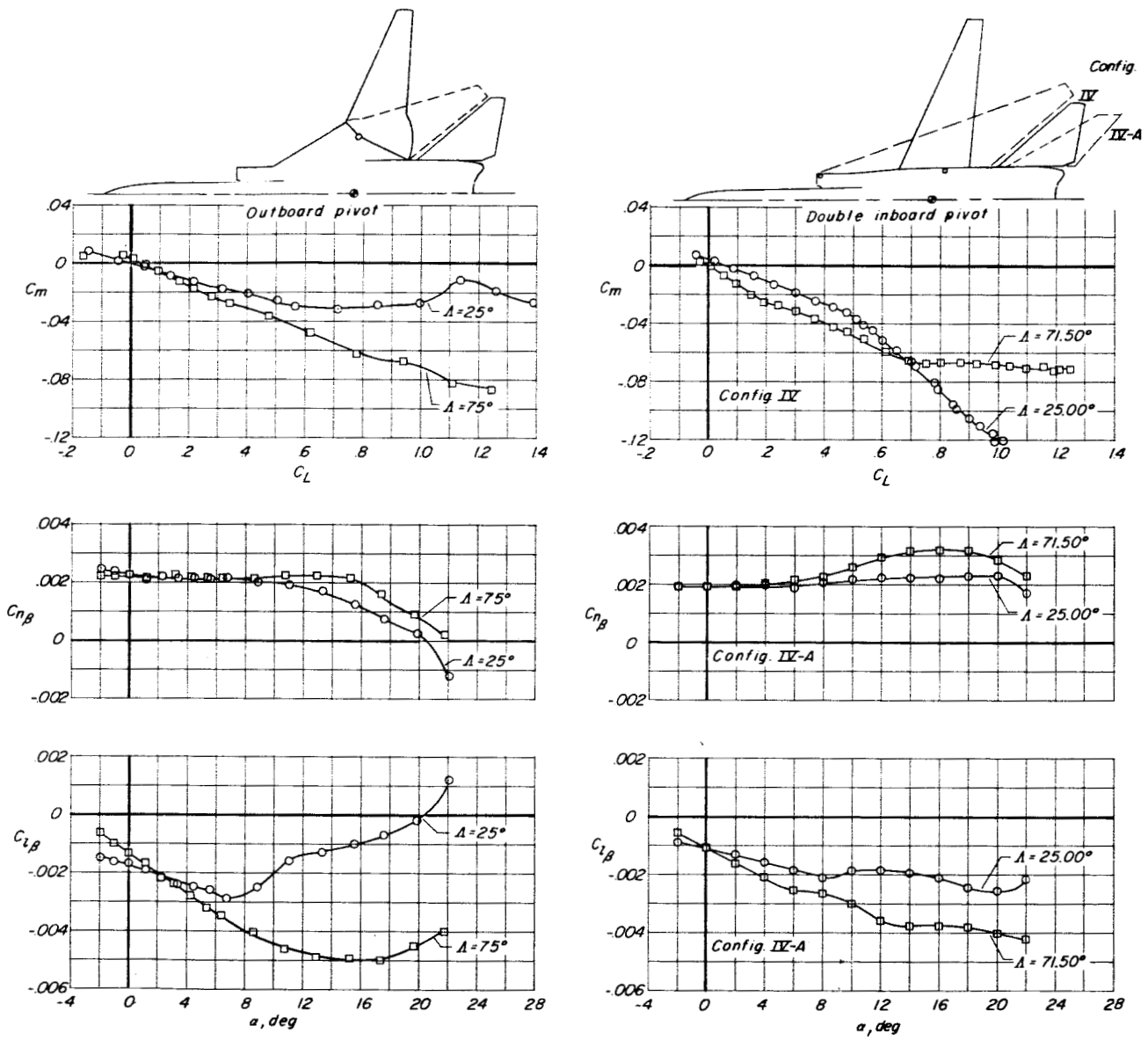

Figure 27.- Comparison of low-speed stability characteristics of outboard-pivot (configuration I of ref. 2) and double-inboard-pivot configurations.